A biophotoelectrochemical approach to unravelling the role of cyanobacterial cell structures in exoelectrogenesis

Laura T. Wey[a], Joshua M. Lawrence[a,b], Xiaolong Chen[b], Robert Clark[a], David J. Lea-Smith[a,1], Jenny Z. Zhang[b,*] & Christopher J. Howe[a,*]

[a]Department of Biochemistry, University of Cambridge, Tennis Court Road, Cambridge CB2 1QW United Kingdom

[b]Yusuf Hamied Department of Chemistry, University of Cambridge, Lensfield Road, Cambridge CB1 2EW United Kingdom

[*]Email: ch26@cam.ac.uk; jz366@cam.ac.uk

---

[1]Present address: School of Biological Sciences, University of East Anglia, Norwich NR4 7TJ, United Kingdom

Abstract

Photosynthetic microorganisms can export electrons outside their cells, a phenomenon called exoelectrogenesis, which can be harnessed for solar energy conversion. However, the route electrons take from thylakoid membranes to the cell exterior is not understood. Electrochemistry is a powerful analytical technique for studying electron transfer pathways. Here, we show how photoelectrochemistry can be used to compare electron flux from cyanobacterial cells of different growth stages, species and with the outer layers systematically removed. We show that the periplasmic space contributes significantly to the photocurrent profile complexity of whole cells, indicating that it gates electron transfer in exoelectrogenesis. We found that although components of the type IV pili machinery do not have a role in exoelectrogenesis, they contribute significantly to cell-electrode adherence. This study establishes that analytical photoelectrochemistry and molecular microbiology provide a powerful combination to study exoelectrogenesis, enabling future studies to answer biological questions and advance solar energy conversion applications.

Keywords: Photosynthetic microorganisms; exoelectrogenesis; analytical photoelectrochemistry; photocurrent output; type IV pili

1. Introduction

Isolated chloroplasts and photosynthetic microorganisms, including eukaryotic algae and cyanobacteria, can export electrons or reducing equivalents upon illumination in a phenomenon called 'exoelectrogenesis'.[1–5] Exoelectrogenesis is a poorly understood process hypothesised to be involved in response to light stress,[6] iron acquisition,[7] or signalling.[8] Despite our lack of understanding of the mechanism, exoelectrogenesis has been demonstrated to be useful for solar energy conversion applications, for example in biophotovoltaics where exoelectrogenic photosynthetic cells are employed to convert sunlight into electricity.[3,9–13] However, gaps in understanding of the mechanism(s) of exoelectrogenesis hinder the development of such novel biotechnologies.

Most studies of the exoelectrogenic activity of cyanobacterial cells have concentrated on the maximum current output under illumination. However, the current output over time under light/dark cycles gives a 'photocurrent profile' with complexity (i.e. a pattern of peaks and troughs before reaching a steady-state) that is not seen using isolated photosystem II (**Fig. 1A**), [10,14–19] which is known to be the initial source of the electrons eventually exported during exoelectrogenesis.[20,21] The molecular basis of this complexity is not known. We hypothesised that it results from the route taken by the electrons from photosystem II across the many outer layers of the cyanobacterial cell structure to the electrode **(Fig. 1B).**

The cell structure of Gram-negative cyanobacteria, such as *Synechocystis sp*. PCC6803 (*Synechocystis*), is well characterised. Photosystem II is a part of the photosynthetic electron transport chain, which is located in the thylakoid membranes in cyanobacteria and other oxygenic photosynthetic organisms. The cyanobacterial thylakoid membranes are separated from the cytoplasmic membrane bounding the cell by the cytoplasm.[22] Outside the cytoplasmic membrane is, collectively referred to as the cell wall, a periplasmic space containing a peptidoglycan layer, an outer membrane, and a surface layer (S-layer) composed of a lattice formed of a single glycoprotein.[23] Extracellular appendages traverse the cytoplasmic membrane and cell wall,[24] including type IV pili, also known as thick pili, which are 6-8 nm in diameter and more than 2 μm long, and are mainly composed of the major pilin pilA1 with possible contributions from minor pilins. There are also thin pili, which are 3-4 nm in diameter and up to 1 μm long but have not been characterised further. There is some evidence of direct extracellular electron transfer via type IV pili,[25,26] but recent genetic and conductivity data call this into question.[18] There is evidence for an endogenous electron mediator (for example, a quinone or NADPH) that enables indirect extracellular electron transfer from the cell to the electrode surface.[16,27,28]

The mechanism of electron transfer by isolated proteins, including photosystem II, has been well studied using electrochemistry.[19,29–32] Here, we apply photoelectrochemistry to study

exoelectrogenesis of cyanobacterial cells **(Fig. 1C)**. To identify the cyanobacterial cell structure gating exoelectrogenesis and thus responsible for the photocurrent profile complexity we analysed the photocurrent output of subcellular fractions of *Synechocystis* cells from which different outer layers had been removed. To do this, we first developed a robust microbiological and analytical protocol for comparing the differences in photocurrent profiles of cyanobacterial cells cultured to different growth phases and from different species. We also investigated the effect of cell-electrode adherence on photocurrent outputs, and tested the longevity and efficiency of connection to electrodes ('wiring') of subcellular fractions. This top-down biophotoelectrochemical approach has allowed us to identify the importance of the periplasmic space in the gating of cyanobacterial extracellular electron transfer.

Approximate location of Figure 1

2. Experimental

2.1. Cell Culture and Growth Conditions

Synechocystis sp. PCC 6803 (*Synechocystis*) and *Synechococcus elongatus sp.* PCC7942 (*Synechococcus*) were cultured photoautotrophically under 50 μmol photons m^{-2} s^{-1} of continuous white light at 30°C in BG11 medium supplemented with 10 mM $NaHCO_3$.[33] Liquid cultures were bubbled with air and shaken at 120 rpm. 1.5% (w/v) agar was used in solid medium. Antibiotics were added at a final concentration of 25 μg ml^{-1} chloramphenicol, 50 μg ml^{-1} kanamycin and 50 μg ml^{-1} apramycin as appropriate. Culture growth was measured by attenuance at 750 nm (OD_{750}). Culture chlorophyll concentration (nmol(Chl *a*) ml^{-1}) was calculated from absorbances at 680 nm and 750 nm: (A_{680}-A_{750}) × 10.814.[34] All measurements were taken using a UV-1800 Spectrophotometer (Shimadzu).

2.2. Pilus mutants

The *Synechocystis* pilus mutants and Wilde Lab wild-type strain[35] were a gift from Prof. Annegret Wilde (University of Freiburg, Germany) and Prof. Conrad Mullineaux (Queen Mary

University of London, UK). The mutant lacking the major pilin (Δ*pilA1*) had the *pilA1* (*sll1694*) gene interrupted with a chloramphenicol resistance cassette.[35] The mutant lacking some of the minor pilins (Δ*pilA9-slr2019*) had the *pilA9-slr2019* operon interrupted with a kanamycin resistance cassette.[36] The mutant lacking the type IV pilus extension mechanism (Δ*pilB1*) used had the *pilB1* gene (*slr0063*) interrupted with a kanamycin resistance cassette, and the hyperpiliated mutant (Δ*pilT1*) had the *pilT1* gene (*slr0161*) interrupted with an apramycin resistance cassette.[35] The genotypes were confirmed by PCR amplification of the interrupted loci in the pilus mutants and the wild-type background using screening primers in Supplementary Table 3, followed by agarose gel electrophoresis of the PCR products.

2.3. Generation of the surface-layer knock out

The surface layer gene (*sll1951*) was disrupted in the Howe Lab wild-type strain of *Synechocystis*[37] to generate a marker-less surface-layer mutant (ΔS-layer) by a method previously described.[38] The genome sequence of *Synechocystis*[39] was consulted via Cyanobase (http://genome.kazusa.or.jp/cyanobase) for primer design. Primers used are listed in Supplementary Table 5 and PCR was performed by standard procedures using Phusion high fidelity DNA polymerase (NEB). Gene deletion of *sll1951* was performed by amplifying an upstream 966bp fragment in the N-terminal region of *sll1951* using primers Sll1951leftfor and Sll1951leftrev and a 954bp downstream fragment in the N-terminal region of *sll1951* using primers Sll1951rightfor and Sll1951rightrev, followed by insertion of the respective fragments into the *Eco*R1/*Bam*HI and *Bam*HI/*Xba*I sites of pUC19 to generate pSll1951-1. The *Bam*HI digested *npt1*/*sacRB* cassette from pUM24Cm[40] was inserted into the *Bam*HI site between the upstream and downstream fragments in pSll1951-1 to generate pSll1951-2. To generate marked mutants approximately 1 µg of pSll1951-1 plasmid was mixed with *Synechocystis* cells for 4 hours in liquid medium, followed by incubation on BG11 agar plates for approximately 24 hours. An additional 3 ml of agar containing kanamycin was added to the surface of the plate followed by further incubation for approximately 1-2 weeks.

Transformants were subcultured to allow segregation of mutant alleles. Segregation was confirmed by PCR using primers Slayer_screen_F and Slayer_screen_R, which flank the deleted region. Generation of unmarked mutants was carried out according to a method previously described.[41] To remove the *npt1/sacRB* cassette, the mutant line was transformed with 1 μg of the markerless pSll1951-2 construct. Following incubation in BG-11 liquid medium for 4 days and agar plates containing sucrose for a further 1-2 weeks, transformants were patched on kanamycin and sucrose plates. Sucrose resistant, kanamycin sensitive strains containing the unmarked deletion were confirmed by PCR amplification using primers Slayer_screen_F and Slayer_screen_R, followed by capillary electrophoresis of the PCR products using a QIAxcel Advanced System (QIAGEN).

2.4. Transmission electron microscopy

The phenotype of the ΔS-layer mutant was confirmed by thin-section and negative stain transmission electron microscopy of newly generated ΔS-layer mutant and wild-type background.

2.5. Preparation of spheroplasts

Spheroplasts were prepared from 50 ml of *Synechocystis* culture of the Howe Lab wild-type strain[37] grown to early stationary phase (OD_{750} = 1.0) according to a previously reported method,[42] with the following alterations: the cell-lysozyme mixture was not sonicated and only incubated for 1 h at 30˚C, and the spheroplasts were harvested by centrifugation at 3000 g for 7 min at room temperature. The formation of spheroplasts was confirmed by resuspending the spheroplast preparation in water and visualising by light microscopy the ghost-like appearance of lysed spheroplasts resulting from the hypo-osmotic shock.[43] As a further test that spheroplasts were prepared, the presence of phycobilin protein was measured by UV-Vis spectroscopy in the supernatant of a spheroplast preparation resuspended in water.

2.6. Thylakoid membrane enrichment

Cyanobacterial thylakoid membranes were enriched from 1 L of *Synechocystis* culture of the Howe Lab wild-type strain[37] grown to early stationary phase (OD_{750} = 1 ± 0.05) according to a

previously reported method,[44] with the exception that the 1mM benzamidine in Buffer A was replaced with a 1x concentration of cOmplete™ Protease Inhibitor Cocktail. The thylakoid membrane enrichment was resuspended to a final volume of 200 µl with a fine brush. The chlorophyll concentration was measured by methanol extraction and UV-Vis spectroscopy, using the extinction co-efficient of Chl a at 665.5 nm in methanol (70020 [mol Chl a]$^{-1}$ dm^3 cm^{-1}).[45]

2.7. Oxygen evolution measurements

Oxygen evolution was measured using a Clark Electrode consisting of an Oxygraph Plus Electrode Control Unit, S1 Oxygen Electrode Disc, DW2/2 Electrode Chamber and a LED1 High Intensity LED Light Source (Hansatech Instruments). Measurements were performed on 1.5 ml samples of each subcellular fraction of *Synechocystis* containing 10 µg ml^{-1} of Chl a in appropriate electrolyte supplemented with 1 mM 2,6-dichloro-1,4-benzoquinone (DCBQ) and 1 mM potassium ferricyanide. Measurements were collected at 25˚C with 1 min darkness, followed by 1 min of 1500 µmol photons m^{-2} s^{-1} light at 627 nm. The rate of oxygen production in the dark was subtracted from that in the light, and normalised to Chl a content. Data were collected from three biological replicates, each with three technical replicates.

2.8. Analytical Photoelectrochemistry

Inverse opal ITO (IO-ITO) electrodes with 10 µm macropores and 3 µm interconnecting channels at a thickness of 40 µm were prepared using the method previously reported.[16]

For wild-type *Synechocystis* and *Synechococcus*, pilus mutants and the ΔS-layer mutant, planktonic cultures of early stationary phase cells at OD$_{750}$ of ca. 1 (unless growth phase stated otherwise) were concentrated by centrifugation at 5000 g for 10 min, the supernatant removed and the pellet resuspended in fresh BG11 medium to a concentration of 150 nmol Chl a ml^{-1}. 250 µL of this solution was dropcast onto the IO-ITO electrodes and left overnight at room temperature in a humid chamber in the dark to allow cell penetration and adhesion, and to minimise the effects of any

differences in light-treatment between batches, yielding cell-loaded electrodes that were used for analysis 16 h later.

For spheroplasts, the final preparation was resuspended in spheroplast buffer to a concentration of 1500 nmol Chl a ml^{-1}. 25 μL of this solution was dropcast onto the IO-ITO electrodes and left for 1 h at room temperature in a humid chamber in the dark to allow spheroplast penetration and adhesion, yielding spheroplast-loaded electrodes which were used immediately for analysis.

For isolated thylakoid membranes, the final preparation was resuspended in thylakoid buffer to a concentration of 225 nmol Chl a ml^{-1}. 10 μL of this solution was dropcast onto the IO-ITO electrodes and left for 15 min at room temperature in a humid chamber in the dark to allow thylakoid membrane penetration and adhesion, yielding thylakoid-loaded electrodes which were used immediately for analysis. This 15 min incubation time is consistent with loading times in previous (photo)electrochemistry studies of protein-films.[16,29,46]

All photoelectrochemical measurements were performed at 25°C using an Ivium Technologies CompactStat, with an Ag/AgCl (saturated) reference electrode (corrected by + 0.197 V for SHE), a platinum mesh counter electrode and loaded IO-ITO working electrode. Chronoamperometry experiments without an exogenous mediator added were performed at an applied potential 0.3 V vs SHE. Chronoamperometry experiments with 1 mM DCBQ exogenous mediator added were performed at an applied potential 0.5 V vs SHE.

Unless otherwise stated, photoelectrochemical measurements were performed in 4.5 ml electrolyte appropriate for the subcellular fraction. The electrolyte for isolated thylakoids was 50 mM MES buffer with, 15 mM NaCl, 5 mM MgCl, 2 mM CaCl$_2$ (pH 6.0); the electrolyte for spheroplasts was 10 mM HEPES buffer with 10 mM MgCl$_2$, 5 mM sodium phosphate and 0.5 M sorbitol (pH 7.5); the electrolyte for whole wild-type cells and mutant cells (ΔSlayer and pilus mutants) was BG11 medium (pH 8.5).

Chronoamperometry experiments were performed at a sampling rate 1 s^{-1}, with light/dark cycles using a collimated LED light source (50 μmol photons m^{-2} s^{-1}, approximately 1 mW cm^{-2} equivalent, 680 nm, Thorlabs). Photocurrent profiles were measured under 60 s light/90 s dark cycles, and when steady-state was reached, the following three photocurrent profiles were taken for analysis. Longevity experiments were performed under 59 min light/1 min dark cycles.

Photocurrents were normalised to the geometric area of the electrode (0.75 cm^2) to obtain photocurrent densities. The Chl a content of the bio-loaded electrode was determined by scraping off the annealed ITO nanoparticles from the FTO coated glass into methanol (500 μL). The suspension was sonicated for 1 h in iced water, then centrifuged at 10 000 g for 3 min. The supernatant was analysed by UV-Vis spectroscopy and the Chl a concentration was determined using the extinction co-efficient of Chl a at 665.5 nm in methanol (70020 [mol Chl a]$^{-1}$ dm^3 cm^{-1}).[45]

For 'wiring' experiments, the photocurrent enhancement with 1 mM DCBQ exogenous mediator added was calculated relative to the photocurrent without an exogenous mediator added. For longevity experiments, the photocurrent at each hour was calculated as a percentage relative to the initial photocurrent.

Three biological replicates of each subcellular fraction were measured. The mean and standard deviation across three biological replicates was calculated. Photocurrent outputs were compared to early stationary phase cells, whole cell or wild-type as appropriate using a one-way one-way analysis of variance (ANOVA) and Tukey's (honestly significant difference) (HSD) test.

2.9. Scanning electron microscopy

Subcellular fractions were loaded onto IO-ITO electrodes and left for a set amount of time under darkness as per the protocol for photoelectrochemistry. The loaded electrodes were rinsed in the electrolyte appropriate for each subcellular fraction. The loaded electrodes were then fixed in liquid nitrogen-cooled ethane and freeze-dried overnight. The loaded electrodes were mounted on aluminium stubs with silver dark and coated with 15 nm iridium using an EMITECH K575X Peltier

cooler. The sample was stored in a desiccator until imaged using a TESCAN MIRA3 FEG-SEM with a 30 kV beam acceleration. Images were processed using Illustrator.

2.10. Confocal fluorescence microscopy

Subcellular fractions were loaded onto bespoke μ-dishes with an IO-ITO electrode on the coverslip bottom and left for a set amount of time under darkness as per the protocol for photoelectrochemistry. The loaded μ-dishes were washed once and then filled with the electrolyte appropriate for the subcellular fraction. The loaded μ-dishes were visualised using a Nikon Eclipse Ti2 Inverted Microscope. Brightfield and autofluorescence of chlorophyll images were taken. Images were processed using NIS Elements Viewer.

2.11. Biofilm formation assay

A crystal violet assay was used to measure biofilm formation as adapted from a protocol previously described for *Synechocystis*.[47] Pilus mutants and wild-type cells of the background used to construct the mutants (the Wilde laboratory strain) were loaded onto ITO-coated polyethylene terephthalate (ITO-PET) 1 cm^2 discs in wells of a 24-well plate and left for under darkness as per the protocol for photoelectrochemistry. 150 μl was aspirated from each well without disturbing the biofilm before gently washing the cell-loaded disc thrice with 750 μl BG11 medium to remove non-adherent cells. Crystal violet solution (250 μl, 0.1% w/v) in dH_2O was pipetted into each well and incubated for 15 min at room temperature. Following this, 200 μL was aspirated from each well and the disc was washed three times with 250 μl dH_2O. 1 ml DMSO was pipetted into each well and the 24-well plate was vigorously shaken for 15 min. The absorbance at 600 nm of the crystal violet in the DMSO supernatant was measured and used as a proxy for the amount of cellular material bound to the ITO-PET.[48] The surface layer mutant and the wild-type cells of the background used to construct the mutant (the Howe laboratory strain) were loaded onto ITO-PET in previously described biophotovoltaic devices[49] and left under 50 μmol photons m^{-2} s^{-1} of continuous white light for five days before performing the crystal violet assay as above.

3. Results

3.1. Photocurrent profile features are conserved in different growth phases and species

To measure the photocurrent profiles of cyanobacteria reproducibly, we first developed a robust microbial and photoelectrochemical protocol. Cells of two widely used model cyanobacterial species *Synechocystis* and *Synechococcus elongatus* PCC7942 (*Synechococcus*) were cultured photoautotrophically in BG11 medium and harvested at specific phases in the growth cycle of cyanobacteria (exponential, early stationary and late stationary). A concentrated cell suspension with 37.5 nmol of chlorophyll was loaded onto electrodes, which were then left in the dark for 16 h. We used state-of-the-art hierarchically structured inverse-opal indium-tin oxide (IO-ITO) electrodes, which boost cell loading and electrochemical signals.[16,17,50]

Chronoamperometry was conducted at an applied potential of +0.1 V vs Ag/AgCl (saturated KCl) reference electrode (equivalent to +0.3 V vs Standard Hydrogen Electrode (SHE). This is the potential at which the maximum photocurrent is reached for whole *Synechocystis* cells as derived from stepped chronoamperometry in a previous study also using IO-ITO electrodes.[16] In another previous study, +0.3 V vs SHE was shown to be the onset potential of electron transfer from isolated PSII to IO-ITO electrodes, because at lower potentials there was a subtractive cathodic current from reduction of O_2 and formation of reactive oxygen species.[29]

During chronoamperometry the current was measured each second enabling resolution of the features in the trace, and the loaded electrodes were exposed to cycles of 680 nm light at 50 µmol photons m^{-2} s^{-1} (approximately 1 mW cm^{-2} equivalent) to drive photosynthesis, followed by dark, for 60 s and 90 s respectively (after which periods the steady-state currents in the light and dark had stabilised). The photocurrent was calculated as the difference between the steady-state currents in the light and dark. The photocurrent was normalised to the geometric area of the electrode to obtain photocurrent densities, enabling comparison of outputs between electrodes. In addition, the chlorophyll content of cells remaining on the electrodes after photoelectrochemistry experiments was

measured and used as a proxy for the amount of biological material participating in exoelectrogenesis, so different biological samples could be compared.

Comparing the photocurrent outputs of photosynthetic microorganisms between studies is difficult. For example, not all studies report the growth phase, which may affect exoelectrogenesis.[3,4] To investigate exoelectrogenesis at different phases in the growth cycle of cyanobacteria, we compared the photoelectrochemistry of cultures of *Synechocystis* at different growth phases: exponential (optical density at 750 nm 0.4 ± 0.05), early stationary ($OD_{750} = 1 \pm 0.05$), and late stationary ($OD_{750} > 1.5$) phase.[51] Under the conditions described above, the cells at the different growth phases gave reproducible photocurrent profiles that were complex (i.e. did not simply reach a steady-state directly) and showed the same features. They all showed two peaks at 5 s and 25 s after illumination, a trough that reached its minimum at 12 s after illumination and a broader trough that reached its minimum at 15 s after the light was turned off (**Fig. 2A, C**). The individual features of the photocurrent profile may be attributable to waves of contribution from different proteins. The peaks and troughs in the photocurrent profile were most pronounced for exponential phase cells. The variation in photocurrent profile between biological replicates was smallest for early stationary phase cells. This could be due to variation among exponential phase cultures with an OD750 ca. 0.4 in the point at which they begin to experience some light limitation, and variation among late-stationary phase cultures in the point at which they begin to adapt differently to their environment or undergo cell death, as observed previously.[34,51]

The photocurrent outputs of the different cells loaded were determined, with exponential phase cells yielding a photocurrent density (0.21 ± 0.03 μA cm^{-2}) approximately double that from early stationary phase cells (0.110 ± 0.004 μA cm^{-2}) (**Fig. 2D**). When normalised to the chlorophyll content, the photocurrent densities of electrodes loaded with cells from exponential, early stationary and late stationary phases were similar (early stationary phase: 160 ± 74 A cm^{-2} mol^{-1}(Chl a)) (**Fig. 2E**). For subsequent analytical photoelectrochemical experiments, cells harvested at early stationary

phase ($OD_{750} = 1 \pm 0.05$) were used, as they displayed the least variability between replicate measurements.

A range of cyanobacterial species have been used in studies of photocurrent output, including in studies of isolated photosynthetic proteins and cells, making it difficult to draw comparisons.[3] To investigate exoelectrogenesis in different model cyanobacterial species, we compared the photoelectrochemistry of early stationary phase cultures of *Synechocystis* and *Synechococcus* under the above protocol. *Synechococcus* yielded photocurrent outputs (raw and chlorophyll-normalised, **Fig 2 D, E**) similar to those of *Synechocystis*. *Synechococcus* also gave a reproducible, complex photocurrent profile that displayed some of the same features as that of *Synechocystis*, although the magnitude of the features in the photocurrent profile varied between the two cyanobacterial species, with the possibility that at least one feature was obscured in *Synechococcus*. The trough recorded at 12 s after illumination was significantly larger in *Synechococcus* than *Synechocystis*, obscuring where there was a peak 25 s after illumination in the photocurrent profile of *Synechocystis* (**Fig. 2B**). To localise the molecular origin of these features, subsequent comparisons of the photoelectrochemistry of subcellular fractions were performed with material derived only from *Synechocystis* cells.

Approximate location of Figure 2

3.2. Preparation of subcellular fractions on IO-ITO electrodes

To identify the role of cyanobacterial cell structure in exoelectrogenesis, specifically to determine which outer layers were responsible for the complexity in the photocurrent profile of whole wild-type cells, we took a top-down approach. We analysed the photoelectrochemistry of subcellular fractions of *Synechocystis* cells, from which different outer layers had been removed (**Supplementary Table 1**).

To investigate the role of extracellular appendages, several previously characterised *Synechocystis* mutants lacking different components of the type IV pili machinery were tested (**Fig.**

3A).[35,36] These include the Δ*pilA1* and Δ*pilA9-slr2019* mutants, which lack some structural major or minor pilins, respectively, and the Δ*pilB1* mutant, which lacks the type IV pili extension motor. Both the Δ*pilA1* and Δ*pilB1* mutants have no thick pili, and the pili of the Δ*pilA9-slr2019* mutant appear like the pili of the wild-type. The Δ*pilT1* mutant was also tested, which is hyperpiliated (i.e. more thick pili than wild-type cells) due to loss of the type IV pili retraction motor. The genotypes of the pilus mutants were confirmed by PCR (**Supplementary Fig. 2**).

To investigate the role of the most peripheral layer of the cell, the surface layer, a *Synechocystis* mutant lacking the surface layer (ΔS-layer) was tested (**Fig. 4A**). The ΔS-layer mutant was generated by using a recombination-based method to disrupt the *sll1951* gene that encodes the protein that solely constitutes the surface layer,[38] and this was confirmed by PCR (Supplementary Fig. 3). Negative stain transmission electron microscopy of thin sections was used to confirm the absence of the surface layer in ΔS-layer cells (**Supplementary Fig. 4**). This showed the cell wall of the ΔS-layer mutant was thinner than that of the wild-type, and the most peripheral layer of the ΔS-layer mutant was smooth like lipopolysaccharide rather than the rougher glycosylated surface-layer present in wild-type cells. The appearance of the mutant was consistent with other mutants generated previously that lack the surface layer.[43]

To investigate the role of the middle layers of the cell wall, spheroplasts, which do not have an intact peptidoglycan layer in the periplasmic space, were tested (**Fig. 4A**). Spheroplasts from Gram-negative bacteria, including cyanobacteria, also have a partial to complete loss of the outer membrane, which reduces the integrity of the periplasmic space in addition to the dissolution of the peptidoglycan layer.[52] To generate spheroplasts from *Synechocystis*, whole wild-type cells from cultures that had reached early stationary phase were given a gentle lysozyme treatment.[42] The preparation of osmotically fragile spheroplasts was confirmed by lysing the preparation in water and detecting phycobiliprotein in the supernatant by UV-Vis spectroscopy (**Supplementary Fig. 5**) and visualising the spheroplast 'ghosts' by light microscopy (**Supplementary Fig. 6**).

We also tested thylakoid membranes from *Synechocystis*, without any cytoplasm or bounding outer layers **(Fig. 4A)**. To isolate thylakoid membranes, whole wild-type cells from cultures that had reached early stationary phase were lysed and the membranes enriched by differential centrifugation of the lysate.[44] Note that electrons would be collected only from the cytoplasmic face of the thylakoid membrane vesicles, so 'inside-out' thylakoid membrane vesicles should not contribute to or decrease the photocurrent output.

To confirm that the subcellular fractions had similar photosystem II activity, which generates the electrons from water oxidation that are eventually exported by the cell in exoelectrogenesis, we measured oxygen evolution. Whole wild-type cells, ΔS-layer mutant cells and spheroplasts showed similar photosystem II activity normalised to chlorophyll (whole wild-type cells: 91 ± 22 $\mu mol(O_2)$ $mg^{-1}(chl)$ h^{-1}). Thylakoid membranes showed lower photosystem II activity (30 ± 6 $\mu mol(O_2)$ $mg^{-1}(chl)$ h^{-1}) (**Supplementary Fig. 7**).

IO-ITO electrodes were loaded with the different subcellular fractions, and the incubation time was individually optimised to allow for penetration and adhesion of the material onto the electrodes. Loaded electrodes were rinsed in electrolyte optimal for each subcellular fraction (**Supplementary Table 2**) to remove excess biological material, then transferred to fresh electrolyte

in the photoelectrochemical cell for chronoamperometry under light/dark cycles. The electrolyte for wild-type and mutant cells (ΔS-layer and pilus mutants) was BG11 medium, the electrolyte for spheroplasts was spheroplast buffer, and the electrolyte for thylakoid membranes was thylakoid buffer.

To confirm the integrity of the different subcellular fractions on the electrodes before photoelectrochemistry experiments, loaded electrodes were visualised by scanning electron microscopy (**Supplementary Fig. 8**). Wild-type and mutant cells (ΔS-layer and pilus mutants) as well as spheroplasts were observed as spheres on the electrodes and thylakoid membranes formed thin films on the surface of the electrodes. To visualise the integration and distribution of the subcellular fractions within the hierarchically structured IO-ITO electrodes, subcellular fractions were loaded on microscopy-dishes with an IO-ITO electrode on the coverslip bottom as per the protocol for photoelectrochemistry experiments. Chlorophyll autofluorescence of the subcellular fractions on the loaded electrodes was visualised by confocal microscopy (**Supplementary Fig. 9**) and confirmed that the subcellular fractions penetrated the IO-ITO electrodes through the channels and pores.

3.3. Type IV pili are involved in cell-electrode adherence but do not contribute to exoelectrogenesis

To investigate whether components of the type IV pili have a role in exoelectrogenesis and the complexity of the photocurrent profile of cells, we measured the photocurrent profile of the different *Synechocystis* pilus mutants (**Fig. 3B**) under the standardised photoelectrochemical conditions used to capture the photocurrent profile of whole wild-type cells (**Fig. 2C**). All the pilus mutants exhibited complex photocurrent profiles similar to those of whole wild-type cells with two peaks at approximately 5 s and 25 s after illumination, a trough that reached its minimum approximately 12 s after illumination, and a broader trough that reached its minimum approximately 15 s after the light was turned off.

The photocurrent outputs of the different *Synechocystis* pilus mutants were calculated from the photocurrent profiles (**Fig. 3C**). The mutants with reduced thick pili yielded significantly lower photocurrent output (e.g. Δ*pilB1* mutant cells approximately four-fold lower at 0.05 ± 0.03 µA cm^{-2}) compared to their background wild-type cells (0.19 ± 0.08 µA cm^{-2}). However, there was no statistically significant difference when the photocurrent outputs were normalised to the chlorophyll content remaining on the electrodes after photoelectrochemistry experiments (**Fig. 3D**).

To determine whether this was due to differences in cell loading, we measured the biofilm formation of wild-type and pilus mutant cells on flat ITO-coated polyethylene terephthalate (ITO-PET) using a crystal violet assay (**Fig. 3E**). The wild-type and hyperpiliated Δ*pilT1* mutant cells had significantly greater biofilm formation on ITO-PET ($Abs_{600} = 0.6 \pm 0.2$ and 0.53 ± 0.06, respectively) than mutants with reduced thick pili (e.g. Δ*pilA1* mutant cells approximately three-fold lower $Abs_{600} = 0.20 \pm 0.03$). This confirms that the type IV pili are important in biofilm formation and surface adherence of *Synechocystis* onto materials, including ITO electrodes. Together with the photocurrent profiles, this indicates that in *Synechocystis* the type IV pili have no role in extracellular electron transfer from the cell to the electrode, but their loss results in lower photocurrent outputs because of a reduction in the number of cells adhering to the electrode.

Approximate location of Figure 3

3.4. The periplasmic space determines the complex photocurrent profile of *Synechocystis* cells

Having shown that the type IV pili extracellular appendages were not responsible for the complexity in the photocurrent profile of cells, we considered the outer layers of the cyanobacterial structure. We measured the photocurrent profile under our standardised photoelectrochemical conditions of the subcellular fractions of *Synechocystis* with different outer layers removed (**Fig. 4B**). The ΔS-layer mutant (no surface layer) exhibited a complex photocurrent profile similar to that of whole wild-type cells. However, there was no difference in raw or chlorophyll-normalised photocurrent outputs between ΔS-layer mutant and the corresponding wild-type cells (**Fig. 4C, D**). Further, the ΔS-layer mutant showed similar amounts of biofilm formation to wild-type cells on ITO-PET (**Supplementary Fig. 10**). Therefore, we concluded that in *Synechocystis* the surface layer does not affect cell-electrode extracellular electron transfer or adherence.

The spheroplasts (with compromised periplasmic space, no peptidoglycan layer and incomplete outer membrane) and isolated thylakoid membranes (no cytoplasmic membrane, peptidoglycan, outer membrane or S-layer) showed monophasic photocurrent profiles under the same experimental regime, with a sharp increase in the current that reached a steady-state a few seconds after illumination, and a sharp decrease in the current that reached a steady-state a few seconds after the light was turned off (**Fig. 4B**). In addition, the steady-state current in the dark was higher in spheroplasts than whole cells. There was no significant difference in chlorophyll-normalised photocurrent densities between spheroplasts or thylakoid membranes and whole cells (**Fig. 4D**). We accounted for differences in photocurrent profile that would be caused by different electrolytes, pH, buffering and loading techniques (**Supplementary Fig. 11-13**). This indicates that the periplasmic space is responsible for the complex features of the photocurrent profile in cells.

Approximate location of Figure 4

3.5. Comparison of wiring efficiency and longevity of subcellular fractions

To determine how directly wired the different subcellular fractions were to the electrodes, we measured the effect of adding an exogenous electron mediator that enables efficient indirect electron transfer from most active photosynthetic electron transport pathways present at the surface of the electrode (independent of the spatial arrangement, for example). We performed the chronoamperometry experiments in the presence of the model mediator 2,6-dichloro-1,4-benzoquinone (DCBQ) at an applied potential of 0.5 V vs SHE for maximal mediation by DCBQ (E_m = 0.315 V vs SHE).[16] We calculated the increase in photocurrent output in the presence of DCBQ relative to the photocurrent without the exogenous mediator added. If the subcellular fraction were poorly wired, then DCBQ would significantly increase the photocurrent output; whereas if the subcellular fraction were already wired well, then DCBQ would have a negligible effect on the photocurrent output. DCBQ gave rise to an approximately 60-fold higher photocurrent output for whole cells, whereas it gave rise to a three-fold higher photocurrent output for enriched thylakoid membranes (**Fig. 5A**). The fact that addition of the exogenous mediator resulted in a bigger increase in photocurrent output for whole cells than for thylakoid membranes indicates that enriched thylakoid membranes were inherently more efficiently wired to the electrodes than whole cells. The wiring of the spheroplasts was intermediate between whole cells and thylakoid membranes. In a previous study also using IO-ITO electrodes, the same concentration of DCBQ gave rise to an approximately two-fold higher photocurrent output for isolated PSII.[16]

To determine the long-term stability of the different subcellular fractions, which is an important consideration in practical applications, we measured the photocurrent outputs of the different subcellular fractions over a 10 h period. We calculated the photocurrent output each hour relative to the initial photocurrent output (**Fig. 5B**). The photocurrent output of whole cells remained approximately the same across the 10 h period, consistent with previous studies.[16] On the other hand, the photocurrent outputs of spheroplasts and thylakoid membranes fell to approximately 30%

of their initial photocurrent outputs by 10 h. Spheroplasts and thylakoid membranes had similar photocurrent output half-lives of approximately 6 h (spheroplasts 49 ± 6 %, thylakoid membrane 56 ± 14% initial photocurrent output at the 6 h). Thylakoids performed similarly to previous studies, likely due to protein degradation or photodamage that could not be repaired outside a living cell.[21] Although one might have expected photocurrent output from spheroplasts to last longer, their performance is consistent with the reported ability of spheroplasts of other bacteria to carry out metabolic reactions for only a few hours and be unable to replicate normally.[53,54]

Approximate location of Figure 5

4. Discussion

In this study, we were able to observe complex photocurrent profiles of cyanobacterial cells reproducibly under standardised microbiological and analytical photoelectrochemical conditions. While complex photocurrent profiles have been recorded in other studies,[10,14–19] drawing comparisons between them is challenging due to the use of different conditions. We kept constant, among other things, the ITO electrode material with an inverse-opal high surface area, the temperature, the intensity and wavelength of light (and used physiologically relevant light intensity), and the amount of chlorophyll loaded onto the electrodes. We also quantified the chlorophyll remaining on the electrodes after experiments, enabling comparison of photocurrent outputs normalised to chlorophyll. We then were able to investigate systematically the effect of growth phase, cyanobacterial species, and outer layers of the cell structure on exoelectrogenesis by varying those parameters in the biological samples we analysed using our robust photoelectrochemistry protocol. We found that the growth phase of the cells did not have a significant effect on exoelectrogenesis. However, the photocurrent profiles of the two different model cyanobacterial species and some subcellular fractions differed.

While the photocurrent profiles of the two model organisms *Synechocystis* and *Synechococcus* exhibit complexity and the same broad features, we observed differences in the magnitudes of their

features. For example, the trough recorded at 12 s after illumination was significantly deeper and broader in *Synechococcus* than *Synechocystis*, engulfing the peak at 25 s after illumination. The exact reason for the difference in their photocurrent profiles remains to be determined as there are many differences between *Synechocystis* and *Synechococcus* and the exact mechanism of exoelectrogenesis remains to be elucidated. A possible explanation is the different shapes of the cells, as *Synechocystis* and *Synechococcus* are spherical and rod-shaped, respectively, and cell morphology has been predicted to have a role in exoelectrogenesis.[55] In addition, while both species are freshwater, *Synechocystis* is moderately halotolerant in comparison to *Synechococcus*, and ion channels have been hypothesised to have a role in exoelectrogenesis.[16,56] Differences in photocurrent profiles of difference cyanobacterial species will be the subject of future studies examining other model organisms.[57]

We observed that spheroplasts, without an intact periplasmic space,[52] yielded a monophasic photocurrent profile distinct from the complex profile of whole cells. This indicates that the periplasmic space contributes significantly to the complexity in the photocurrent profile of whole cells and likely acts as a gate for electron flow. The periplasmic space in *Synechocystis* contains redox active metabolites[58] and proteins involved in reductive metal acquisition[59], such as FutA2, which binds Fe^{3+} prior to uptake by the FutB/C plasma membrane transporter and is also proposed to be involved in copper-transport,[60,61] and CopM, which binds Cu^+.[62] There is evidence that reductive iron acquisition is linked to the respiratory terminal oxidases,[63] and both iron acquisition and oxidase activity have been shown to be involved in exoelectrogenesis.[6,7] In addition, the periplasmic space bounded by the outer membrane provides a controlled environment on the extracellular side of the plasma membrane, which contains many proteins and a plastoquinol pool from the partial respiratory electron transfer chain.[59,64,65] Future studies should examine the role of individual components of the periplasmic space, and periplasmic-dependent components of the plasma membrane, on exoelectrogenesis in *Synechocystis*.

We also observed that enriched thylakoid membranes yielded a monophasic photocurrent profile, similar to that of isolated photosystem II reported using similar conditions.[16] Isolated photosystem II from cyanobacteria has been shown to participate in direct electron transfer to IO-ITO electrodes,[46] and isolated thylakoid membranes from plants such as spinach have also been shown to participate in direct electron transfer to carbon paper electrodes.[21,66,67] It seems likely that the photosystems in the enriched thylakoid membranes from cyanobacteria are functioning similarly. Previous electrochemical studies of cyanobacterial thylakoid membranes have shown electron transport to the electrode in the absence of exogenous mediators. However, the exact mechanism of electron transfer to the electrode was not characterised.[68,69] Future studies should use analytical photoelectrochemistry to study further the electron transfer from cyanobacterial thylakoid membranes to electrodes to inform us about not only the photosynthetic electron transport chain, but also the co-localised respiratory electron transport chain and other redox reactions that occur in the cyanobacterial thylakoid membranes.

Cyanobacterial exoelectrogenesis has long been hypothesised to involve a contribution from direct extracellular electron transfer via type IV pili.[3,16,65] Previous atomic force microscopy (AFM) studies, including by Gorby *et al.*, reported that *Synechocystis* type IV pili are electrically conductive.[25,26] The pili of the heterotrophic exoelectrogen *Geobacter sp.* have been shown to be electrically conductive, although these are much smaller in diameter than those in *Synechocystis*, which also lack the hyper-aromaticity that facilitates conductivity.[70–72] Another recent study by Thirumurthy *et al.* showed that *Synechocystis* type IV pili are not required for extracellular electron transfer, as mutant cells lacking type IV pili due to deletion of the *pilD* pilin gene (and another mutation in a *pilA* pilin protein processing gene) yielded similar photocurrent output to wild-type cells on a carbon cloth electrode.[18] Further, the authors reported that the *Synechocystis* type IV pili are not electrically conductive as measured by AFM, although the sample was not under low inorganic carbon conditions as described by Gorby *et al.*.[25] In this study, we observed that a

variety of pilus mutant cells yielded complex photocurrent profiles and similar photocurrent outputs (normalised to chlorophyll content) compared to wild-type cells. Therefore, we concluded that type IV pili, including major and minor pilins or the type IV pili retraction and extension mechanisms, do not contribute to exoelectrogenesis in *Synechocystis*, confirming the study by Thirumurthy *et al.*.[18] In addition, in this study we also observed that the surface layer did not contribute to or impede exoelectrogenesis in *Synechocystis*.

It remains to be determined if cyanobacterial exoelectrogenesis involves a contribution from direct extracellular electron transfer via non-pilus or surface-layer cell features. Heterotrophic exoelectrogens such as *Geobacter* sp., *Shewanella oneidensis* and *Pseudomonas putida* are known to have redox metabolites and proteins in their extracellular polysaccharide matrices.[73,74] In this study we did not specifically investigate the extracellular polysaccharide matrix, but this will be a subject of future studies.

Nevertheless, we found that the cell surface features of *Synechocystis* affected the cell loading on the electrodes. *Synechocystis* is known to live as a planktonic species, as well as undergoing flocculation or biofilm formation.[24,47] Type IV pili have been shown to have a role in biofilm formation in heterotrophic bacteria such as *Pseudomonas aeruginosa*.[75,76] In cyanobacteria, type IV pili have been shown to have a role in aggregation and flocculation.[35,77] Type IV pili have been shown not to be involved in biofilm formation in *Synechococcus*,[78] but involved in *Synechocystis* biofilm formation,[47] when grown on glass, which is nonphysiological and not an electrode material. In this study, we observed that mutant cells with reduced thick pili were less adherent than wild-type or hyperpiliated cells on ITO electrode materials. Previous attempts to increase BPV outputs have focused on optimising the electrode and biological materials separately, for example. Our results suggest that future attempts should explore optimising the cell-electrode interface, including increasing cell adherence to the electrode and therefore increasing loading and decreasing the fragility of electrodes, reducing loss of non-adherent cells when

operating. The hyperpiliated Δ*pilT1* mutant is a promising candidate, as are other mutants genetically engineered to have greater biofilm formation.[79]

The wiring efficiency of whole cells to electrodes could also be improved. Previous benchmark power outputs in two-electrode biophotovoltaic devices and photocurrent density outputs in three-electrode photoelectrochemical set-ups have come from increasing wiring through exogenous mediators, such as quinones,[13,80] phenazines[81] or potassium ferricyanide,[9,82] or redox polymers.[83,84] However such exogenous mediators give rise to a redox potential drop during the electron transfer process, and may be cytotoxic and unsuitable for large-scale applications.[81,85] We have shown here that by modifying the outer layers of the cell structure the wiring can be improved, as we found that spheroplasts had intermediate wiring between whole cells and thylakoid membranes. However, spheroplasts did not maintain the good long-term stability of whole cells.

5. Conclusion

This study demonstrated that the application of analytical photoelectrochemistry to study the detailed photocurrent profiles of a systematic set of microbiological samples is an effective approach for dissecting the role of biological components in exoelectrogenesis. We showed that the periplasmic space significantly contributed to the complex photocurrent profile cells, but the surface layer or thick type IV pili did not. This supports the existence of an endogenous electron mediator that facilitates indirect extracellular electron transfer from *Synechocystis* cells to the electrode. This approach opens up many possibilities for dissecting the role of specific biological components in extracellular electron transfer events by exoelectrogenic cells.

and Prof. Conrad Mullineaux (Queen Mary University of London, UK) for the gift of the pilus mutants used in this study and discussion about their phenotypes.

Appendix A. Supplementary materials

Supplementary data associated with this article can be found, in the online version.

References

[1]   W. Haehnel, H.J. Hochheimer, On the current generated by a galvanic cell driven by photosynthetic electron transport, J. Electroanal. Chem. 104 (1979) 563–574. https://doi.org/10.1016/S0022-0728(79)81069-4.

[2]   H. Ochiai, H. Shibata, Y. Sawa, T. Katoh, "Living electrode" as a long-lived photoconverter for biophotolysis of water., Proc. Natl. Acad. Sci. U. S. A. 77 (1980) 2442–4. https://doi.org/10.1073/PNAS.77.5.2442.

[3]   L.T. Wey, P. Bombelli, X. Chen, J.M. Lawrence, C.M. Rabideau, S.J.L. Rowden, J.Z. Zhang, C.J. Howe, The Development of Biophotovoltaic Systems for Power Generation and Biological Analysis, ChemElectroChem. 6 (2019) 5375–5386. https://doi.org/10.1002/celc.201900997.

[4]   J. Tschörtner, B. Lai, J.O. Krömer, Biophotovoltaics: Green Power Generation From Sunlight and Water, Front. Microbiol. 10 (2019) 866. https://doi.org/10.3389/fmicb.2019.00866.

[5]   M. Grattieri, K. Beaver, E.M. Gaffney, F. Dong, S.D. Minteer, Advancing the fundamental understanding and practical applications of photo-bioelectrocatalysis, Chem. Commun. 56 (2020) 8553–8568. https://doi.org/10.1039/d0cc02672g.

[6] R.W. Bradley, P. Bombelli, D.J. Lea-Smith, C.J. Howe, Terminal oxidase mutants of the cyanobacterium Synechocystis sp. PCC 6803 show increased electrogenic activity in biological photo-voltaic systems, Phys. Chem. Chem. Phys. 15 (2013) 13611–13618. https://doi.org/10.1039/c3cp52438h.

[7] A.C. Gonzalez-Aravena, K. Yunus, L. Zhang, B. Norling, A.C. Fisher, Tapping into cyanobacteria electron transfer for higher exoelectrogenic activity by imposing iron limited growth, RSC Adv. 8 (2018) 20263–20274. https://doi.org/10.1039/C8RA00951A.

[8] A. Prindle, J. Liu, M. Asally, S. Ly, J. Garcia-Ojalvo, G.M. Süel, Ion channels enable electrical communication in bacterial communities, Nature. 527 (2015) 59–63. https://doi.org/10.1038/nature15709.

[9] K.L. Saar, P. Bombelli, D.J. Lea-Smith, T. Call, E.-M. Aro, T. Müller, C.J. Howe, T.P.J. Knowles, Enhancing power density of biophotovoltaics by decoupling storage and power delivery, Nat. Energy. 3 (2018) 75–81. https://doi.org/10.1038/s41560-017-0073-0.

[10] M. Sawa, A. Fantuzzi, P. Bombelli, C.J. Howe, K. Hellgardt, P.J. Nixon, Electricity generation from digitally printed cyanobacteria, Nat. Commun. 8 (2017) 1327. https://doi.org/10.1038/s41467-017-01084-4.

[11] A.J. McCormick, P. Bombelli, A.M. Scott, A.J. Philips, A.G. Smith, A.C. Fisher, C.J. Howe, Photosynthetic biofilms in pure culture harness solar energy in a mediatorless bio-photovoltaic cell (BPV) system, Energy Environ. Sci. 4 (2011) 4699–4709. https://doi.org/10.1039/c1ee01965a.

[12] C.J. Howe, P. Bombelli, Electricity Production by Photosynthetic Microorganisms, Joule. 4 (2020) 2065–2069. https://doi.org/10.1016/j.joule.2020.09.003.

[13] G. Longatte, F. Rappaport, F.A. Wollman, M. Guille-Collignon, F. Lemaître, Electrochemical Harvesting of Photosynthetic Electrons from Unicellular Algae Population at the Preparative Scale by Using 2,6-dichlorobenzoquinone, Electrochim. Acta. 236 (2017) 337–342.

https://doi.org/10.1016/j.electacta.2017.03.124.

[14] J.M. Pisciotta, Y. Zou, I. V. Baskakov, Light-Dependent Electrogenic Activity of Cyanobacteria, PLoS One. 5 (2010) e10821. https://doi.org/10.1371/journal.pone.0010821.

[15] A. Cereda, A. Hitchcock, M.D. Symes, L. Cronin, T.S. Bibby, A.K. Jones, A Bioelectrochemical Approach to Characterize Extracellular Electron Transfer by Synechocystis sp. PCC6803, PLoS One. 9 (2014) 91484. https://doi.org/10.1371/journal.pone.0091484.

[16] J.Z. Zhang, P. Bombelli, K.P. Sokol, A. Fantuzzi, A.W. Rutherford, C.J. Howe, E. Reisner, Photoelectrochemistry of Photosystem II in Vitro vs in Vivo, J. Am. Chem. Soc. 140 (2018) 6–9. https://doi.org/10.1021/jacs.7b08563.

[17] T. Wenzel, D. Härtter, P. Bombelli, C.J. Howe, U. Steiner, Porous translucent electrodes enhance current generation from photosynthetic biofilms, Nat. Commun. 9 (2018) 1299. https://doi.org/10.1038/s41467-018-03320-x.

[18] M.A. Thirumurthy, A. Hitchcock, A. Cereda, J. Liu, M.S. Chavez, B.L. Doss, R. Ros, M. El-Naggar, J.T. Heap, T. Bibby, A.K. Jones, Type IV Pili-Independent Photocurrent Production by the cyanobacterium Synechocystis sp. PCC 6803, Front. Microbiol. 11 (2020) 1344. https://doi.org/10.3389/FMICB.2020.01344.

[19] J.Z. Zhang, E. Reisner, Advancing photosystem II photoelectrochemistry for semi-artificial photosynthesis, Nat. Rev. Chem. 4 (2020) 6–21. https://doi.org/10.1038/s41570-019-0149-4.

[20] J.M. Pisciotta, Y. Zou, I. V. Baskakov, Role of the photosynthetic electron transfer chain in electrogenic activity of cyanobacteria, Appl. Microbiol. Biotechnol. 91 (2011) 377–385. https://doi.org/10.1007/s00253-011-3239-x.

[21] P. Bombelli, R.W. Bradley, A.M. Scott, A.J. Philips, A.J. McCormick, S.M. Cruz, A. Anderson, K. Yunus, D.S. Bendall, P.J. Cameron, J.M. Davies, A.G. Smith, C.J. Howe, A.C. Fisher, Quantitative analysis of the factors limiting solar power transduction by Synechocystis

sp. PCC 6803 in biological photovoltaic devices, Energy Environ. Sci. 4 (2011) 4690–4698. https://doi.org/10.1039/c1ee02531g.

[22] A. Rast, M. Schaffer, S. Albert, W. Wan, S. Pfeffer, F. Beck, J.M. Plitzko, J. Nickelsen, B.D. Engel, Biogenic regions of cyanobacterial thylakoids form contact sites with the plasma membrane, Nat. Plants. 5 (2019) 436–446. https://doi.org/10.1038/s41477-019-0399-7.

[23] E. Hoiczyk, A. Hansel, Cyanobacterial cell walls: News from an unusual prokaryotic envelope, J. Bacteriol. 182 (2000) 1191–1199. https://doi.org/10.1128/JB.182.5.1191-1199.2000.

[24] N. Schuergers, A. Wilde, Appendages of the Cyanobacterial Cell, Life. 5 (2015) 700–715. https://doi.org/10.3390/life5010700.

[25] Y.A. Gorby, S. Yanina, J.S. McLean, K.M. Rosso, D. Moyles, A. Dohnalkova, T.J. Beveridge, I.S. Chang, B.H. Kim, K.S. Kim, D.E. Culley, S.B. Reed, M.F. Romine, D.A. Saffarini, E.A. Hill, L. Shi, D.A. Elias, D.W. Kennedy, G. Pinchuk, K. Watanabe, S. Ishii, B. Logan, K.H. Nealson, J.K. Fredrickson, Electrically conductive bacterial nanowires produced by Shewanella oneidensis strain MR-1 and other microorganisms, Proc. Natl. Acad. Sci. 103 (2006) 11358–11363. https://doi.org/10.1073/pnas.0604517103.

[26] S. Sure, A.A.J.J. Torriero, A. Gaur, L.H. Li, Y. Chen, C. Tripathi, A. Adholeya, M.L. Ackland, M. Kochar, Inquisition of Microcystis aeruginosa and Synechocystis nanowires: characterization and modelling, Antonie van Leeuwenhoek, Int. J. Gen. Mol. Microbiol. 108 (2015) 1213–1225. https://doi.org/10.1007/s10482-015-0576-2.

[27] G. Saper, D. Kallmann, F. Conzuelo, F. Zhao, T.N. Tóth, V. Liveanu, S. Meir, J. Szymanski, A. Aharoni, W. Schuhmann, A. Rothschild, G. Schuster, N. Adir, Live cyanobacteria produce photocurrent and hydrogen using both the respiratory and photosynthetic systems, Nat. Commun. 9 (2018) 2168. https://doi.org/10.1038/s41467-018-04613-x.

[28] Y. Shlosberg, B. Eichenbaum, T.N. Tóth, G. Levin, V. Liveanu, G. Schuster, N. Adir,

NADPH performs mediated electron transfer in cyanobacterial-driven bio-photoelectrochemical cells, IScience. 24 (2021) 101892. https://doi.org/10.1016/J.ISCI.2020.101892.

[29] J.Z. Zhang, K.P. Sokol, N. Paul, E. Romero, R. van Grondelle, E. Reisner, Competing charge transfer pathways at the photosystem II–electrode interface, Nat. Chem. Biol. 12 (2016) 1046–1052. https://doi.org/10.1038/nchembio.2192.

[30] F. Zhao, S. Hardt, V. Hartmann, H. Zhang, M.M. Nowaczyk, M. Rögner, N. Plumeré, W. Schuhmann, F. Conzuelo, Light-induced formation of partially reduced oxygen species limits the lifetime of photosystem 1-based biocathodes, Nat. Commun. 9 (2018). https://doi.org/10.1038/s41467-018-04433-z.

[31] F.A. Armstrong, H.A. Heering, J. Hirst, Reaction of complex metalloproteins studied by protein-film voltammetry, Chem. Soc. Rev. 26 (2004) 169. https://doi.org/10.1039/cs9972600169.

[32] C. Léger, P. Bertrand, Direct Electrochemistry of Redox Enzymes as a Tool for Mechanistic Studies, Chem. Rev. 108 (2008) 2379–2438. https://doi.org/10.1021/cr0680742.

[33] R.Y. Stanier, R. Kunisawa, M. Mandel, G. Cohen-Bazire, Purification and properties of unicellular blue-green algae (order Chroococcales)., Bacteriol. Rev. 35 (1971) 171–205. https://doi.org/10.1128/mmbr.35.2.171-205.1971.

[34] D.J. Lea-Smith, N. Ross, M. Zori, D.S. Bendall, J.S. Dennis, S.A. Scott, A.G. Smith, C.J. Howe, Thylakoid terminal oxidases are essential for the cyanobacterium Synechocystis sp. PCC 6803 to survive rapidly changing light intensities., Plant Physiol. 162 (2013) 484–95. https://doi.org/10.1104/pp.112.210260.

[35] F.D. Conradi, R.Q. Zhou, S. Oeser, N. Schuergers, A. Wilde, C.W. Mullineaux, Factors controlling floc formation and structure in the cyanobacterium Synechocystis sp. strain PCC 6803, J. Bacteriol. 201 (2019) e00344-19. https://doi.org/10.1128/JB.00344-19.

[36] T. Wallner, L. Pedroza, K. Voigt, V. Kaever, A. Wilde, The cyanobacterial phytochrome 2 regulates the expression of motility-related genes through the second messenger cyclic di-GMP., Photochem. Photobiol. Sci. 19 (2020) 631–643. https://doi.org/10.1039/c9pp00489k.

[37] J.G.K. Williams, [85] Construction of specific mutations in photosystem II photosynthetic reaction center by genetic engineering methods in Synechocystis 6803, Methods Enzymol. 167 (1988) 766–778. https://doi.org/10.1016/0076-6879(88)67088-1.

[38] D.J. Lea-Smith, R. Vasudevan, C.J. Howe, Generation of marked and markerless mutants in model cyanobacterial species, J. Vis. Exp. 2016 (2016) 540013791–54001. https://doi.org/10.3791/54001.

[39] T. Kaneko, S. Sato, H. Kotani, A. Tanaka, E. Asamizu, Y. Nakamura, N. Miyajima, M. Hirosawa, M. Sugiura, S. Sasamoto, T. Kimura, T. Hosouchi, A. Matsuno, A. Muraki, N. Nakazaki, K. Naruo, S. Okumura, S. Shimpo, C. Takeuchi, T. Wada, A. Watanabe, M. Yamada, M. Yasuda, S. Tabata, Sequence analysis of the genome of the unicellular cyanobacterium Synechocystis sp. strain PCC6803. II. Sequence determination of the entire genome and assignment of potential protein-coding regions., DNA Res. 3 (1996) 109–36. http://www.ncbi.nlm.nih.gov/pubmed/8905231 (accessed November 3, 2017).

[40] J.L. Ried, A. Collmer, An nptI-sacB-sacR cartridge for constructing directed, unmarked mutations in Gram-negative bacteria by marker exchange-eviction mutagenesis, Gene. 57 (1987) 239–246. https://doi.org/10.1016/0378-1119(87)90127-2.

[41] H. Xu, D. Vavilin, C. Funk, W. Vermaas, Multiple Deletions of Small Cab-like Proteins in the Cyanobacterium Synechocystis sp. PCC 6803: CONSEQUENCES FOR PIGMENT BIOSYNTHESIS AND ACCUMULATION, J. Biol. Chem. 279 (2004) 27971–27979. https://doi.org/10.1074/JBC.M403307200.

[42] H. Mi, T. Endo, U. Schreiber, T. Ogawa, K. Asada, NAD(P)H dehydrogenase-dependent cyclic electron flow around photosystem I in the cyanobacterium synechocystis PCC 6803: A

study of dark-starved cells and spheroplasts, Plant Cell Physiol. 35 (1994) 163–173. https://doi.org/10.1093/oxfordjournals.pcp.a078580.

[43] C. Trautner, W.F.J. Vermaas, The sll1951 Gene Encodes the Surface Layer Protein of Synechocystis sp. Strain PCC 6803, J. Bacteriol. 195 (2013) 5370–5380. https://doi.org/10.1128/JB.00615-13.

[44] J. Komenda, J. Barber, Comparison of psbO and psbH Deletion Mutants of Synechocystis PCC 6803 Indicates that Degradation of D1 Protein Is Regulated by the QB Site and Dependent on Protein Synthesis, Biochemistry. 34 (1995) 9625–9631. https://doi.org/10.1021/bi00029a040.

[45] Y. Li, N. Scales, R.E. Blankenship, R.D. Willows, M. Chen, Extinction coefficient for red-shifted chlorophylls: chlorophyll d and chlorophyll f, Biochim. Biophys. Acta -Bioenergetics. 1817 (2012) 1292–1298. https://doi.org/10.1016/j.bbabio.2012.02.026.

[46] K.P. Sokol, D. Mersch, V. Hartmann, J.Z. Zhang, M.M. Nowaczyk, M. Rögner, A. Ruff, W. Schuhmann, N. Plumeré, E. Reisner, Rational wiring of photosystem II to hierarchical indium tin oxide electrodes using redox polymers, Energy Environ. Sci. 9 (2016) 3698–3709. https://doi.org/10.1039/c6ee01363e.

[47] R. Allen, B.E. Rittmann, R. Curtiss, Axenic biofilm formation and aggregation by synechocystis sp. Strain PCC 6803 are induced by changes in nutrient concentration and require cell surface structures, Appl. Environ. Microbiol. 85 (2019) e02192-18. https://doi.org/10.1128/AEM.02192-18.

[48] G.A. O'Toole, Microtiter dish Biofilm formation assay, J. Vis. Exp. 47 (2010) 2437. https://doi.org/10.3791/2437.

[49] T.P. Call, T. Carey, P. Bombelli, D.J. Lea-Smith, P. Hooper, C.J. Howe, F. Torrisi, Platinum-free, graphene based anodes and air cathodes for single chamber microbial fuel cells, J. Mater. Chem. A. 5 (2017) 23872–23886. https://doi.org/10.1039/C7TA06895F.

[50] D. Mersch, C.-Y.Y. Lee, J.Z. Zhang, K. Brinkert, J.C. Fontecilla-Camps, A.W. Rutherford, E. Reisner, Wiring of Photosystem II to Hydrogenase for Photoelectrochemical Water Splitting, J. Am. Chem. Soc. 137 (2015) 8541–8549. https://doi.org/10.1021/jacs.5b03737.

[51] R.M. Schuurmans, J.C.P. Matthijs, K.J. Hellingwerf, Transition from exponential to linear photoautotrophic growth changes the physiology of Synechocystis sp. PCC 6803, Photosynth. Res. 132 (2017) 69–82. https://doi.org/10.1007/s11120-016-0329-8.

[52] M.D. Berliner, D. Neely-Fisher, B.H. Rosen, R.W. Fisher, Spheroplast induction in Anabaena variabilis Kütz and A. azollae stras, Protoplasma. 139 (1987) 36–40. https://doi.org/10.1007/BF01417533.

[53] U. Taubeneck, J. Gumpert, Some notes on gram-negative bacteria with experimentally altered surface structures, Folia Microbiol. (Praha). 12 (1967) 258–263. https://doi.org/10.1007/BF02868741.

[54] Z.A. McGee, R.G. Wittler, H. Gooder, P. Charache, Wall-Defective Microbial Variants: Terminology and Experimental Design, J. Infect. Dis. 123 (1971) 433–438. https://doi.org/10.1093/infdis/123.4.433.

[55] T.I. Okedi, A.C. Fisher, K. Yunus, Quantitative analysis of the effects of morphological changes on extracellular electron transfer rates in cyanobacteria, Biotechnol. Biofuels. 13 (2020) 150. https://doi.org/10.1186/s13068-020-01788-8.

[56] N. Pade, M. Hagemann, Salt acclimation of cyanobacteria and their application in biotechnology, Life. 5 (2015) 25–49. https://doi.org/10.3390/life5010025.

[57] G.A.R. Gale, A.A. Schiavon Osorio, L.A. Mills, B. Wang, D.J. Lea-Smith, A.J. McCormick, Emerging Species and Genome Editing Tools: Future Prospects in Cyanobacterial Synthetic Biology, Microorganisms. 7 (2019) 409. https://doi.org/10.3390/microorganisms7100409.

[58] L.A. Mills, A.J. Mccormick, D.J. Lea-Smith, Current knowledge and recent advances in understanding metabolism of the model cyanobacterium Synechocystis sp. PCC 6803, Biosci.

Rep. 40 (2020) BSR20193325. https://doi.org/10.1042/BSR20193325.

[59] L.L. Baers, L.M. Breckels, L.A. Mills, L. Gatto, M.J. Deery, T.J. Stevens, C.J. Howe, K.S. Lilley, D.J. Lea-Smith, Proteome mapping of a cyanobacterium reveals distinct compartment organization and cell-dispersed metabolism, Plant Physiol. 181 (2019) 1721–1738. https://doi.org/10.1104/pp.19.00897.

[60] A. Badarau, S.J. Firbank, K.J. Waldron, S. Yanagisawa, N.J. Robinson, M.J. Banfield, C. Dennison, FutA2 is a ferric binding protein from Synechocystis PCC 6803, J. Biol. Chem. 283 (2008) 12520–12527. https://doi.org/10.1074/jbc.M709907200.

[61] J. Giner-Lamia, L. López-Maury, J.C. Reyes, F.J. Florencio, The CopRS two-component system is responsible for resistance to copper in the cyanobacterium Synechocystis sp. PCC 6803, Plant Physiol. 159 (2012) 1806–1818. https://doi.org/10.1104/pp.112.200659.

[62] J. Giner-Lamia, L. López-Maury, F.J. Florencio, CopM is a novel copper-binding protein involved in copper resistance in Synechocystis sp. PCC 6803, Microbiologyopen. 4 (2015) 167–185. https://doi.org/10.1002/mbo3.231.

[63] C. Kranzler, H. Lis, O.M. Finkel, G. Schmetterer, Y. Shaked, N. Keren, Coordinated transporter activity shapes high-affinity iron acquisition in cyanobacteria, ISME J. 8 (2014) 409–417. https://doi.org/10.1038/ismej.2013.161.

[64] F. Huang, I. Parmryd, F. Nilsson, A.L. Persson, H.B. Pakrasi, B. Andersson, B. Norling, Proteomics of Synechocystis sp. strain PCC 6803: identification of plasma membrane proteins., Mol. Cell. Proteomics. 1 (2002) 956–66. https://doi.org/10.1074/MCP.M200043-MCP200.

[65] D.J. Lea-Smith, P. Bombelli, R. Vasudevan, C.J. Howe, Photosynthetic, respiratory and extracellular electron transport pathways in cyanobacteria, Biochim. Biophys. Acta - Bioenerg. 1857 (2016) 247–255. https://doi.org/10.1016/j.bbabio.2015.10.007.

[66] M. Rasmussen, S.D. Minteer, Investigating the mechanism of thylakoid direct electron

transfer for photocurrent generation, Electrochim. Acta. 126 (2014) 68–73. https://doi.org/10.1016/J.ELECTACTA.2013.06.081.

[67] D. Pankratov, G. Pankratova, L. Gorton, Thylakoid membrane–based photobioelectrochemical systems: Achievements, limitations, and perspectives, Curr. Opin. Electrochem. 19 (2020) 49–54. https://doi.org/10.1016/j.coelec.2019.09.005.

[68] R.I. Pinhassi, D. Kallmann, G. Saper, S. Larom, A. Linkov, A. Boulouis, M.A. Schöttler, R. Bock, A. Rothschild, N. Adir, G. Schuster, Photosynthetic membranes of Synechocystis or plants convert sunlight to photocurrent through different pathways due to different architectures, PLoS One. 10 (2015) e0122616. https://doi.org/10.1371/journal.pone.0122616.

[69] S. Larom, D. Kallmann, G. Saper, R. Pinhassi, A. Rothschild, H. Dotan, G. Ankonina, G. Schuster, N. Adir, The Photosystem II D1-K238E mutation enhances electrical current production using cyanobacterial thylakoid membranes in a bio-photoelectrochemical cell, Photosynth. Res. 126 (2015) 161–169. https://doi.org/10.1007/s11120-015-0075-3.

[70] F. Wang, Y. Gu, J.P. O'Brien, S.M. Yi, S.E. Yalcin, V. Srikanth, C. Shen, D. Vu, N.L. Ing, A.I. Hochbaum, E.H. Egelman, N.S. Malvankar, Structure of Microbial Nanowires Reveals Stacked Hemes that Transport Electrons over Micrometers, Cell. 177 (2019) 361–369. https://doi.org/10.1016/j.cell.2019.03.029.

[71] D.E. Holmes, Y. Dang, D.J.F. Walker, D.R. Lovley, The electrically conductive pili of Geobacter species are a recently evolved feature for extracellular electron transfer, Microb. Genomics. 2 (2016) e000072. https://doi.org/10.1099/mgen.0.000072.

[72] D.R. Lovley, D.J.F. Walker, Geobacter Protein Nanowires, Front. Microbiol. 10 (2019). https://doi.org/10.3389/fmicb.2019.02078.

[73] S.W. Li, G.P. Sheng, Y.Y. Cheng, H.Q. Yu, Redox properties of extracellular polymeric substances (EPS) from electroactive bacteria, Sci. Rep. 6 (2016) 1–7. https://doi.org/10.1038/srep39098.

[74] D.M. Gurumurthy, R.N. Bharagava, A. Kumar, B. Singh, M. Ashfaq, G.D. Saratale, S.I. Mulla, EPS bound flavins driven mediated electron transfer in thermophilic Geobacillus sp., Microbiol. Res. 229 (2019) 126324. https://doi.org/10.1016/J.MICRES.2019.126324.

[75] G.A. O'Toole, R. Kolter, Flagellar and twitching motility are necessary for Pseudomonas aeruginosa biofilm development, Mol. Microbiol. 30 (1998) 295–304. https://doi.org/10.1046/j.1365-2958.1998.01062.x.

[76] M. Klausen, A. Aaes-Jørgensen, S. Molin, T. Tolker-Nielsen, Involvement of bacterial migration in the development of complex multicellular structures in Pseudomonas aeruginosa biofilms, Mol. Microbiol. 50 (2003) 61–68. https://doi.org/10.1046/j.1365-2958.2003.03677.x.

[77] M. del M. Aguilo-Ferretjans, R. Bosch, R.J. Puxty, M. Latva, V. Zadjelovic, A. Chhun, D. Sousoni, M. Polin, D.J. Scanlan, J.A. Christie-Oleza, Pili allow dominant marine cyanobacteria to avoid sinking and evade predation, Nat. Commun. 12 (2021) 1857. https://doi.org/10.1038/s41467-021-22152-w.

[78] E. Nagar, S. Zilberman, E. Sendersky, R. Simkovsky, E. Shimoni, D. Gershtein, M. Herzberg, S.S. Golden, R. Schwarz, Type 4 pili are dispensable for biofilm development in the cyanobacterium Synechococcus elongatus, Environ. Microbiol. 19 (2017) 2862–2872. https://doi.org/10.1111/1462-2920.13814.

[79] M. Agostoni, C.M. Waters, B.L. Montgomery, Regulation of biofilm formation and cellular buoyancy through modulating intracellular cyclic di-GMP levels in engineered cyanobacteria, Biotechnol. Bioeng. 113 (2016) 311–319. https://doi.org/10.1002/bit.25712.

[80] N. Sekar, Y. Umasankar, R.P. Ramasamy, Photocurrent generation by immobilized cyanobacteria via direct electron transport in photo-bioelectrochemical cells, Phys. Chem. Chem. Phys. 16 (2014) 7862–7871. https://doi.org/10.1039/c4cp00494a.

[81] E.R. Clifford, R.W. Bradley, L.T. Wey, J.M. Lawrence, X. Chen, C.J. Howe, J.Z. Zhang,

Phenazines as model low-midpoint potential electron shuttles for photosynthetic

bioelectrochemical systems, Chem. Sci. 12 (2021) 3328–3338.

https://doi.org/10.1039/d0sc05655c.

[82]   K. Hasan, H. Bekir Yildiz, E. Sperling, P. Ó Conghaile, M.A. Packer, D. Leech, C. Hägerhäll,

L. Gorton, Photo-electrochemical communication between cyanobacteria (Leptolyngbia sp.)

and osmium redox polymer modified electrodes, Phys. Chem. Chem. Phys. 16 (2014) 24676–

24680. https://doi.org/10.1039/C4CP04307C.

[83]   L. Liu, S. Choi, Self-sustainable, high-power-density bio-solar cells for lab-on-a-chip

applications, Lab Chip. 17 (2017) 3817–3825. https://doi.org/10.1039/c7lc00941k.

[84]   V.M. Luimstra, S.-J.J. Kennedy, J. Güttler, S.A. Wood, D.E. Williams, M.A. Packer, A cost-

effective microbial fuel cell to detect and select for photosynthetic electrogenic activity in

algae and cyanobacteria, J. Appl. Phycol. 26 (2014) 15–23. https://doi.org/10.1007/s10811-

013-0051-2.

[85]   G. Longatte, A. Sayegh, J. Delacotte, F. Rappaport, F.-A. Wollman, M. Guille-Collignon, F.

Lemaître, Investigation of photocurrents resulting from a living unicellular algae suspension

with quinones over time, Chem. Sci. 9 (2018) 8271–8281.

https://doi.org/10.1039/C8SC03058H.
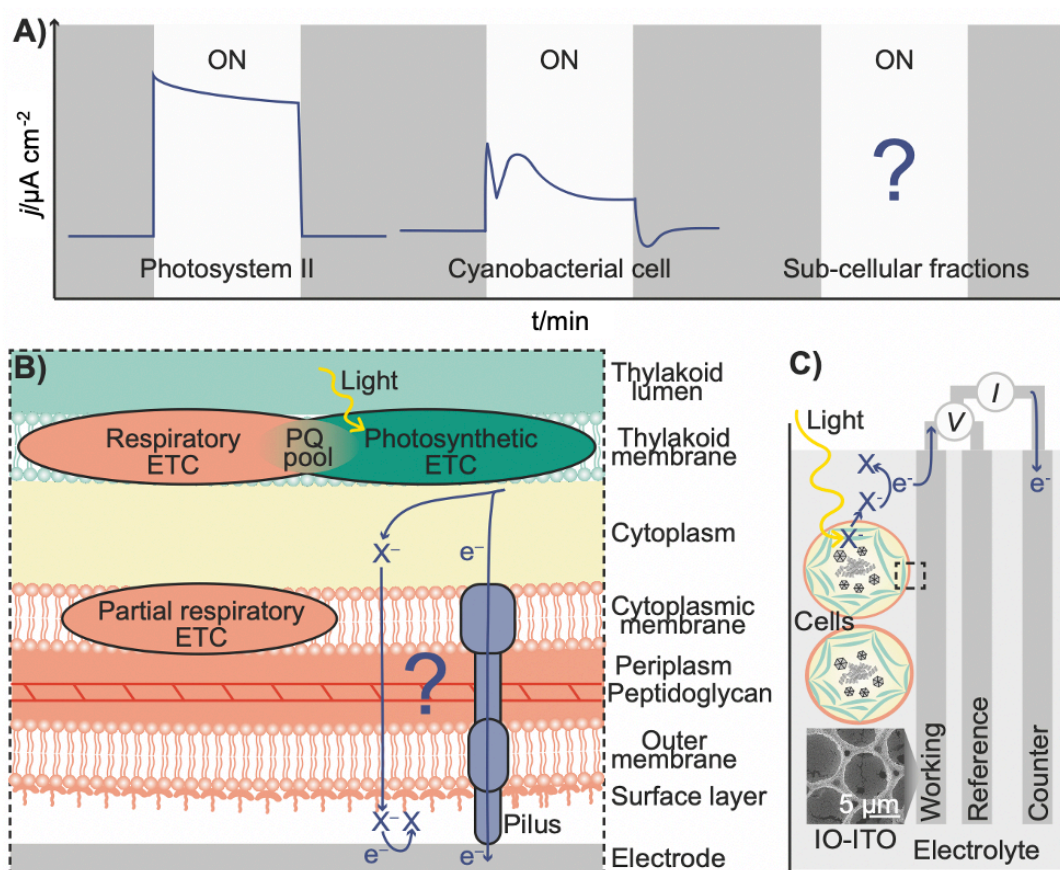
Figure 1 A) Schematic representation of chronoamperometric traces under light/dark cycles (i.e. photocurrent profiles) of photosystem II (PSII) protein-films and biofilms of cyanobacterial cells from previous studies.[16] ON, light on. **B)** Schematic representation of the cell-electrode interface (dashed box from panel C, rotated 90˚) showing cyanobacterial cell topology. Postulated electron transfer pathways behind exoelectrogenesis are shown by purple arrows. 'X' is an unidentified electron carrier produced and exported by the cells under illumination. More detail of the electron transfer pathways is in Supplementary Figure 1. **C)** Schematic representation of the three-electrode photoelectrochemical set-up used for studying exoelectrogenesis. Cyanobacterial cells or subcellular fractions are interfaced with the working electrode which is referenced to the Ag/AgCl electrode. The panel also shows a scanning electron micrograph of an inverse-opal indium tin oxide (IO-ITO) working electrode used in this study.
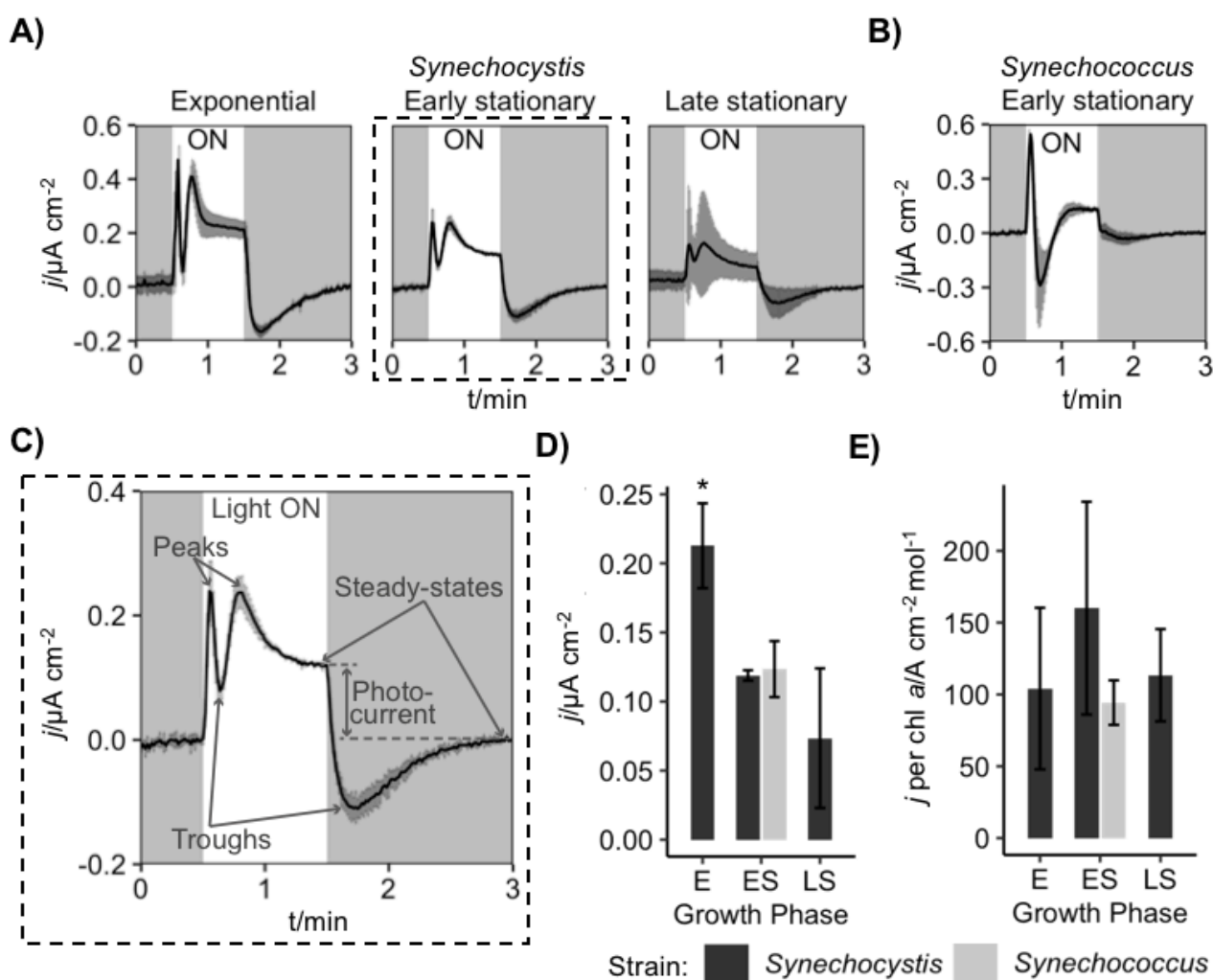
Figure 2 Photocurrent profiles of **A)** *Synechocystis* cells at different growth phases, **B)** *Synechococcus* cells at early stationary phase, and **C)** *Synechocystis* cells at early stationary phase (dashed box from panel A) with features labelled. ON = light on. Photocurrent outputs from *Synechocystis* cells at different growth phases and *Synechococcus* cells at early stationary phase **D)** calculated from photocurrent profiles in panels A and B, and **E)** normalised to chlorophyll (Chl *a*) content of cells remaining on the electrodes after photoelectrochemistry experiments. E = exponential, ES = early stationary, LS = late stationary. All chronoamperometry measurements were recorded at an applied potential of 0.3 V vs. SHE, and under atmospheric conditions at 25 °C in BG11 medium electrolyte. Light conditions used: $\lambda = 680$ nm, 50 µmol photons m^{-2} s^{-1} (approximately 1 mW cm^{-2} equivalent). Data presented as mean ± standard deviation of three

biological replicates, * = P < 0.05 compared to *Synechocystis* cells at early stationary phase using a

one-way ANOVA and Tukey HSD.
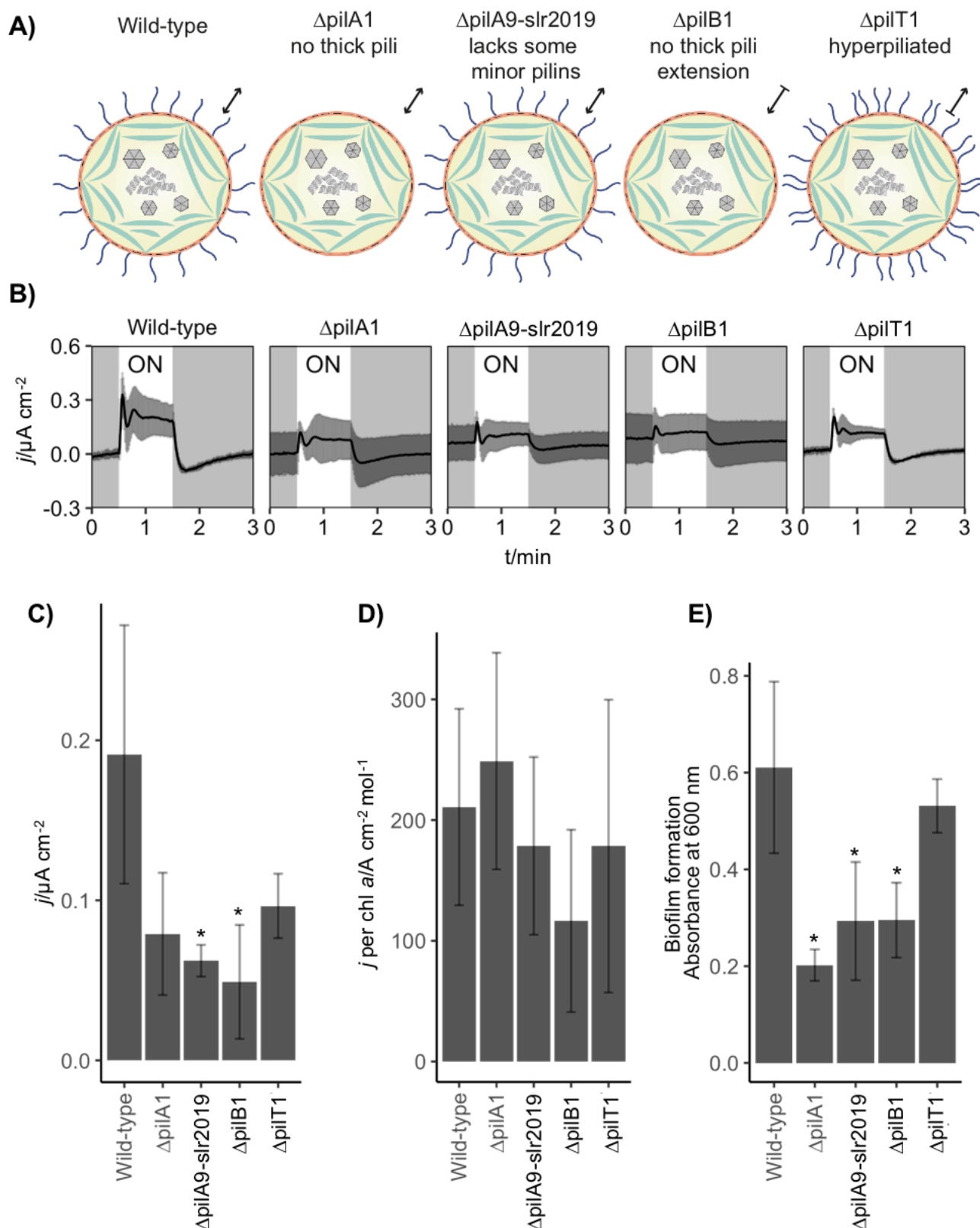
Figure 3 A) Schematic representation of *Synechocystis* pilus mutants with different components of

the type IV pili machinery analysed in this study: wild-type cells, ΔpilA1 mutant cells lacking thick

pili, ΔpilA9-slr2019 mutant cells lacking some minor pilins, ΔpilB1 mutant cells lacking thick pili,

and ΔpilT1 mutant cells that are hyperpiliated. Arrow indicates function of the type IV pili extension/retraction mechanism. **B)** Photocurrent profiles of *Synechocystis* pilus mutants. ON = light on. Photocurrent outputs from *Synechocystis* pilus mutants **C)** calculated from photocurrent profiles in panel B, and **D)** normalised to chlorophyll (Chl *a*) content of cells remaining on the electrodes after photoelectrochemistry experiments. All chronoamperometry measurements were recorded at an applied potential of 0.3 V vs. SHE, and under atmospheric conditions at 25 °C in BG11 medium electrolyte. Light conditions used: $\lambda = 680$ nm, 50 μmol photons m^{-2} s^{-1} (approximately 1 mW cm^{-2} equivalent). **E)** Crystal violet assay of biofilm formation by *Synechocystis* pilus mutants loaded as per the protocol for photoelectrochemistry on ITO-PET. Data presented as mean ± standard deviation of three biological replicates for photoelectrochemistry and four biological replicates for biofilm assay, * = P < 0.05 compared to Wild-type using a one-way ANOVA and Tukey HSD.
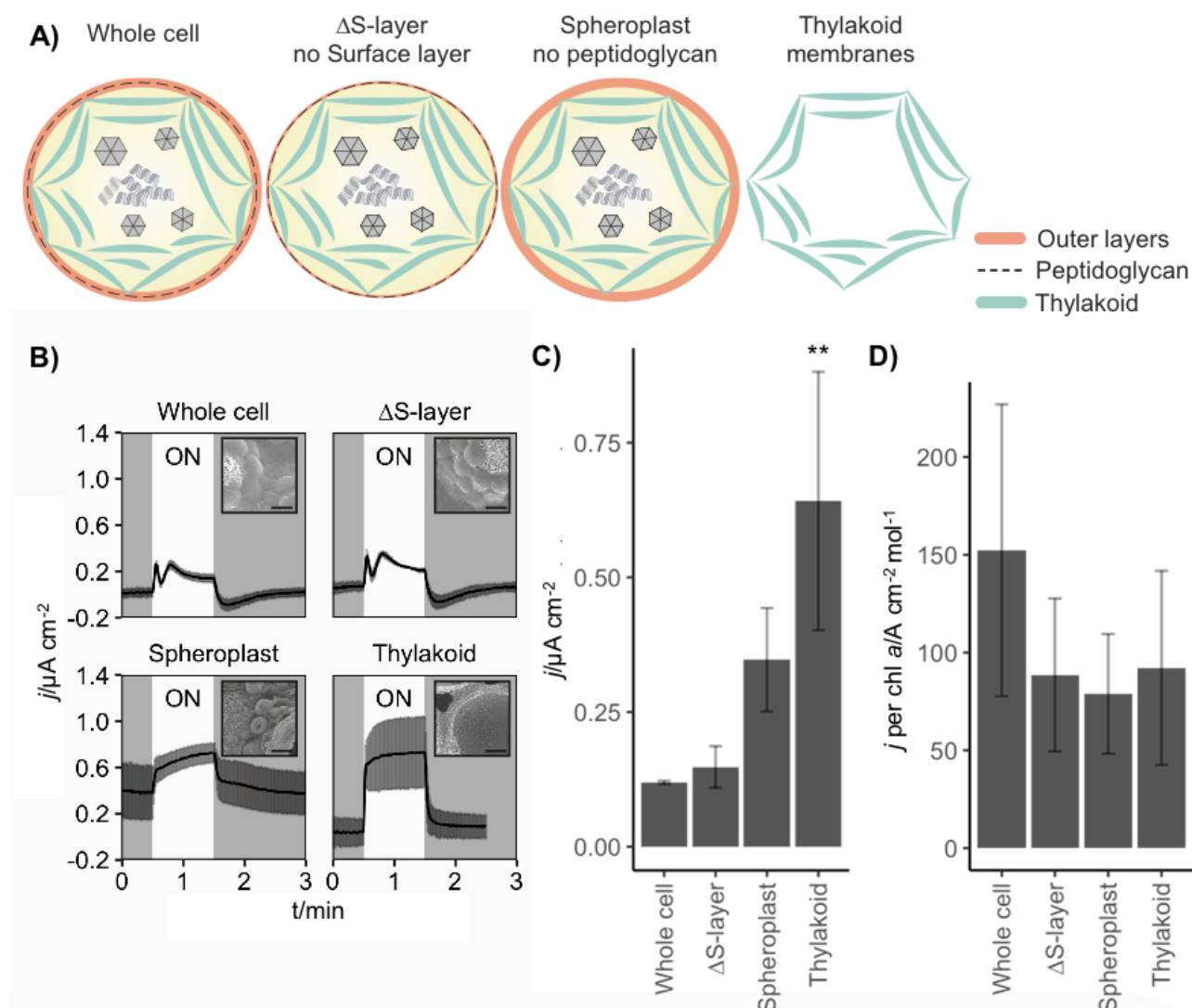
Figure 4 A) Schematic representation of subcellular fractions of *Synechocystis* cells analysed in this study: whole cells, mutant cells lacking the Surface layer (ΔS-layer); spheroplasts without peptidoglycan, and at least partial loss of the outer membrane and periplasmic space; and enriched thylakoid membranes. Pili are not depicted for clarity. **B)** Photocurrent profiles of subcellular fractions of *Synechocystis*. ON = light on. Inserts are scanning electron micrographs of each subcellular fraction loaded onto an IO-ITO electrode. Scale bar is 2 μm. Photocurrent outputs from subcellular fractions of *Synechocystis* **C)** calculated from photocurrent profiles in panel B, and **D)** normalised to chlorophyll (Chl *a*) content of cells remaining on the electrodes after photoelectrochemistry experiments. All chronoamperometry measurements were recorded at an applied potential of 0.3 V vs. SHE, and under atmospheric conditions at 25 °C in BG11 medium

electrolyte for whole cells and ΔS-layer cells, spheroplast buffer for spheroplasts, and thylakoid

buffer for thylakoid membranes . Light conditions used: $\lambda = 680$ nm, 50 µmol photons m^{-2} s^{-1}

(approximately 1 mW cm^{-2} equivalent). Data presented as mean ± standard deviation of three

biological replicates, ** = $P < 0.01$ compared to whole cells using a one-way ANOVA and Tukey

HSD.
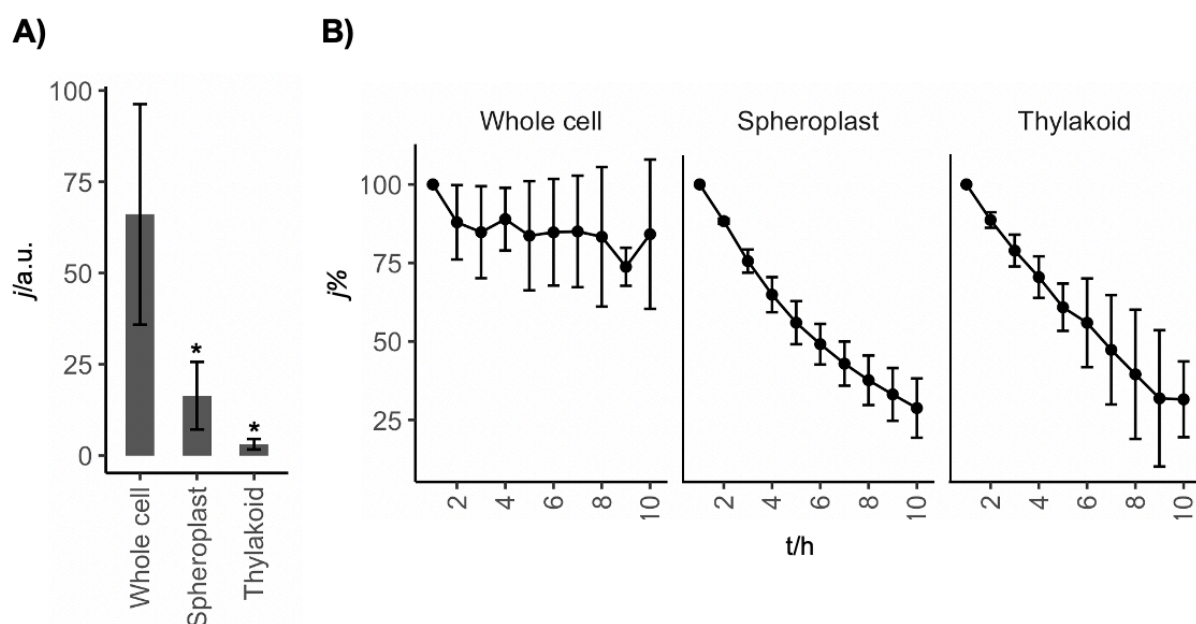
Figure 5 A) Photocurrent outputs from subcellular fractions of *Synechocystis* with DCBQ (1 mM) electron mediator relative to their photocurrent output with no exogenous mediator added as 1 arbitrary unit (a.u.). Chronoamperometry measurements with DCBQ were recorded at an applied potential of 0.5 V vs. SHE. Data presented as mean ± standard deviation of three biological replicates, * = P < 0.05 compared to whole cells using a one-way ANOVA and Tukey HSD. **B)** Photocurrent outputs from subcellular fractions of *Synechocystis* over 10 h as a percentage of the initial photocurrent output. Longevity chronoamperometry measurements were recorded at an applied potential of 0.3 V vs. SHE. Data presented as mean ± standard deviation of three biological replicates. All chronoamperometry measurements were recorded under atmospheric conditions at 25 °C in BG11 medium electrolyte for whole cells, spheroplast buffer for spheroplast and thylakoid buffer for thylakoid membranes. Light conditions used: λ = 680 nm, 50 μmol photons m^{-2} s^{-1} (approximately 1 mW cm^{-2} equivalent).

Supplementary Materials

A biophotoelectrochemical approach to unravelling the role of cyanobacterial cell structures in exoelectrogenesis

Laura T. Wey[a], Joshua M. Lawrence[a,b], Xiaolong Chen[b], Robert Clark[a], David J. Lea-Smith[a,2], Jenny Z. Zhang[b*] & Christopher J. Howe[a*]

[a]Department of Biochemistry, University of Cambridge, Tennis Court Road, Cambridge CB2 1QW United Kingdom

[b]Yusuf Hamied Department of Chemistry, University of Cambridge, Lensfield Road, Cambridge CB1 2EW United Kingdom

[*]Email: ch26@cam.ac.uk; jz366@cam.ac.uk

[2]Present address: School of Biological Sciences, University of East Anglia, Norwich NR4 7TJ, United Kingdom
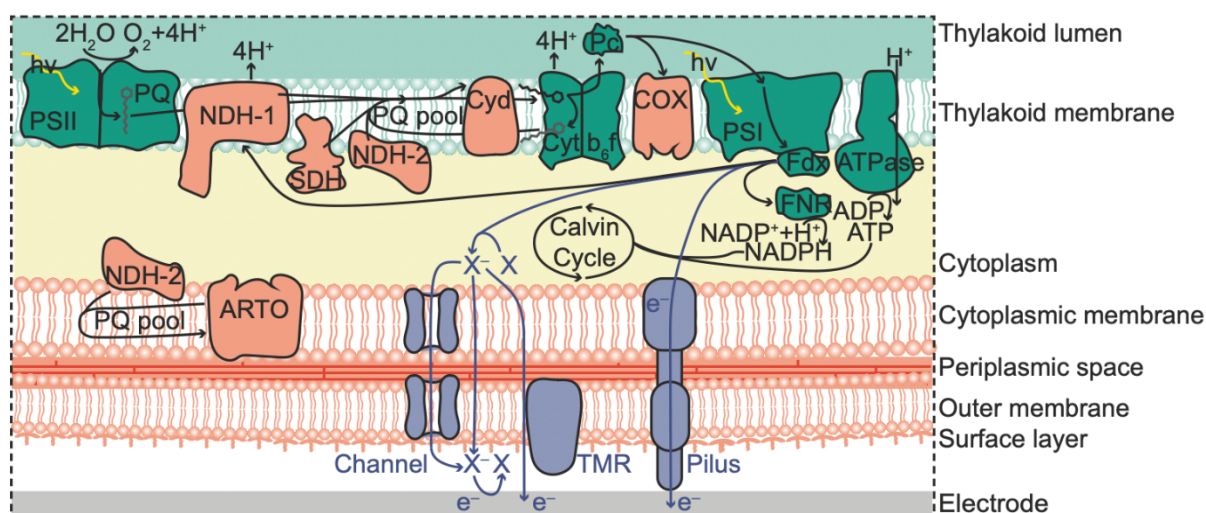
Supplementary Figure 1 Schematic representation of the cell-electrode interface with arrows indicating the electron transfer (ET) pathways: known intracellular (black arrows)[1,2] and postulated ET pathways behind exoelectrogenesis (purple arrows).[3] 'X' is an unidentified electron carrier produced and exported by the cyanobacterial cells under illumination. Postulated mechanisms include electrons stemming from downstream of photosystem I (PSI) and passing to the outside of the cell via channels, passive diffusion, a putative transmembrane reductase (TMR), or type IV pili. Linear photosynthetic electron transport chain proteins (coloured green) are intermingled with the proteins (coloured orange) of the cyclic and respiratory electron transport chains in the thylakoid membrane, and there is a partial respiratory chain in the cytoplasmic membrane. The cell is bounded by the cell wall consisting of the cytoplasmic membrane, outer membrane, and surface layer. Type IV pili traverse these layers of the cell wall. The cytoplasmic and outer membranes are separated by a periplasmic space including the peptidoglycan layer. Proteins: Photosystem II (PSII), NAD(P)H dehydrogenase-like complexes 1 and 2 (NDH-1, -2), cytochrome b_6f complex (Cyt b_6f), plastocyanin (Pc), photosystem I (PSI), ferredoxin (Fdx), ferredoxin-NADP$^+$ reductase (FNR), ATP synthase (ATPase), cytochrome bd-quinol oxidase (Cyd), cytochrome-c oxidase complex (COX), alternative respiratory terminal oxidase (ARTO). Membrane-bound mediators: plastoquinone/ plastoquinol (PQ/PQH$_2$). Phycobilisomes and flavodiiron proteins are not shown for clarity.

Supplementary Table 1 The sub-cellular fractions of *Synechocystis* prepared for photoelectrochemistry analysis in this study.

| Whole wild-type cells starting material	Sub-cellular fraction	Description	Method of preparation	Ref.
Howe Group strain[4]	ΔS-layer mutant cells	Cells lacking the surface layer	Genetic removal of part of the *sll1951* gene that encodes the surface-layer protein	[5]
	Spheroplasts	Cells lacking an intact peptidoglycan layer in the periplasmic space	Gentle lysozyme treatment of whole wild-type cells	[6]
	Thylakoid membranes	Isolated thylakoid membranes	Thylakoid membranes enriched by differential centrifugation of wild-type cell lysate	[7]
Wilde Group strain[8]	ΔpilA1 mutant cells	Cells lacking thick pili	Genetic removal of the *pilA1* (*sll1694*) gene that encodes the major pilin structural protein	[8]
	ΔpilA9-slr2019 mutant cells	Cells lacking some minor pilins	Genetic removal of the *pilA9-slr2019* operon that encodes some of the minor pilin structural proteins	[9]
	ΔpilB1 mutant cells	Cells lacking thick pili	Genetic removal of the *pilB1* (*slr0063*) gene that encodes the type IV pili extension motor	[8]
	ΔpilT1 mutant cells	Hyperpiliated cells	Genetic removal of the *pilT1* (*slr0161*) gene that encodes the type IV pili retraction motor	[8]
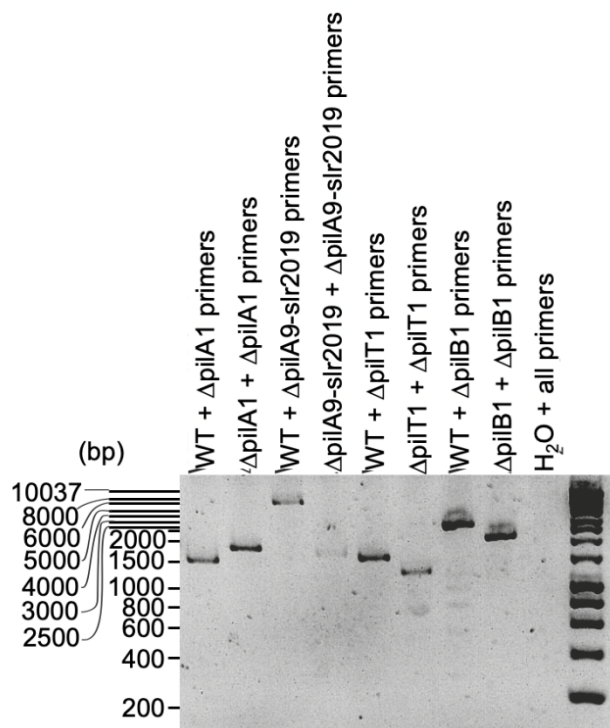
Supplementary Figure 2 Agarose gel from electrophoresis of PCR products from amplification of the pilus gene locus in wild type and pilus mutant strains with appropriate primers (Supplementary Table 3). A negative control of autoclaved dH$_2$O with all primers was used to demonstrate the lack of contamination. Far right lane is Bioline HyperLadder™ 1kb. All bands are at expected size (Supplementary Table 4).
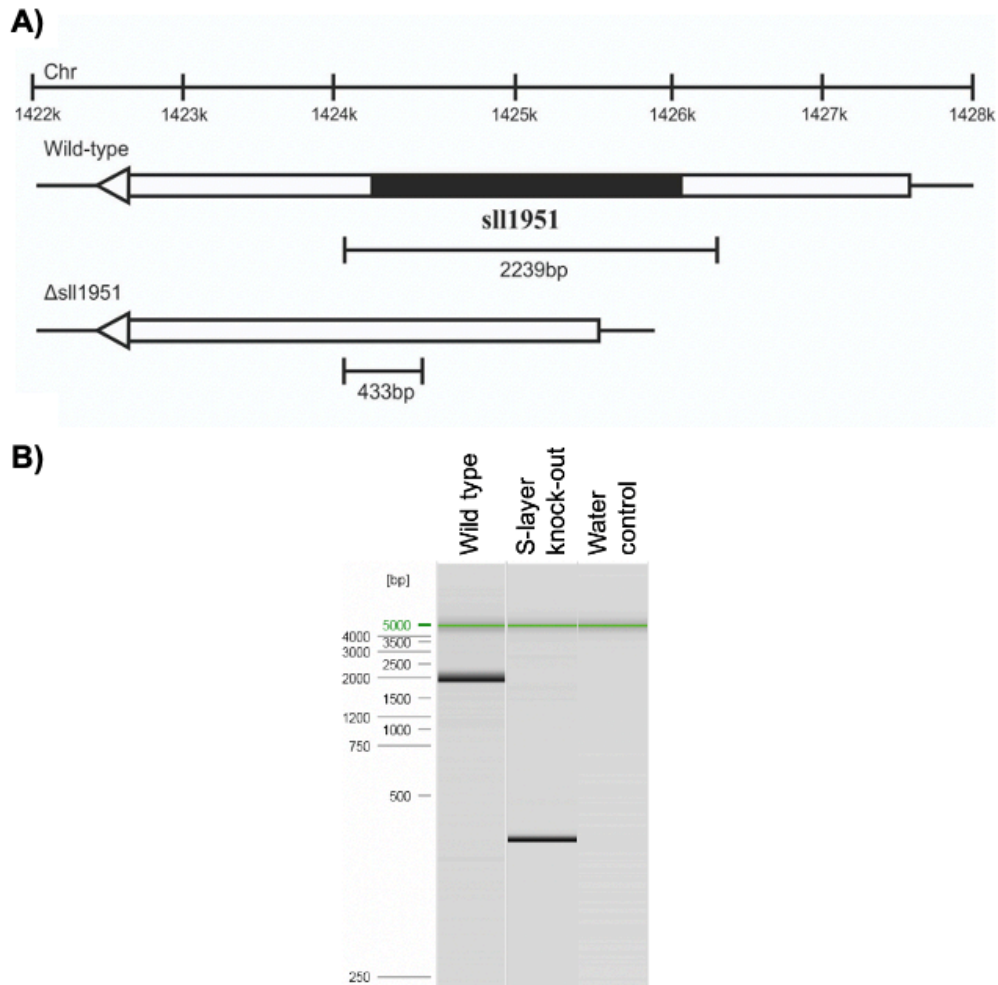
Supplementary Figure 3 A) Schematic representation of locus location in the *Synechocystis* genome (top) and the wild-type (middle) and unmarked surface layer knockout (bottom) profiles expected following amplification with primers flanking the deleted sequence. The region deleted in the mutant strain is shaded in black. **B)** Simulated gel from QIAxcel capillary electrophoresis of PCR products from amplification of the surface-layer gene locus in wild type and surface layer knock-out strains by primers Slayer_screen_F and Slayer_screen_R (Supplementary Table 5). The size of band expected for the wild type cells was 2239 bp and for the knock out 433 bp.
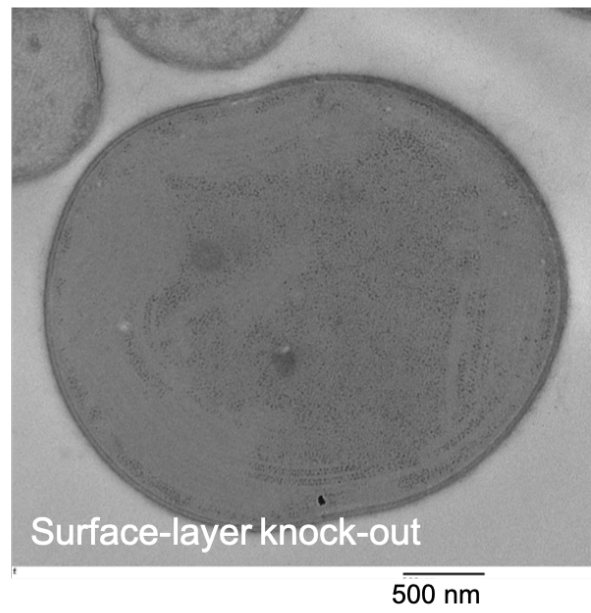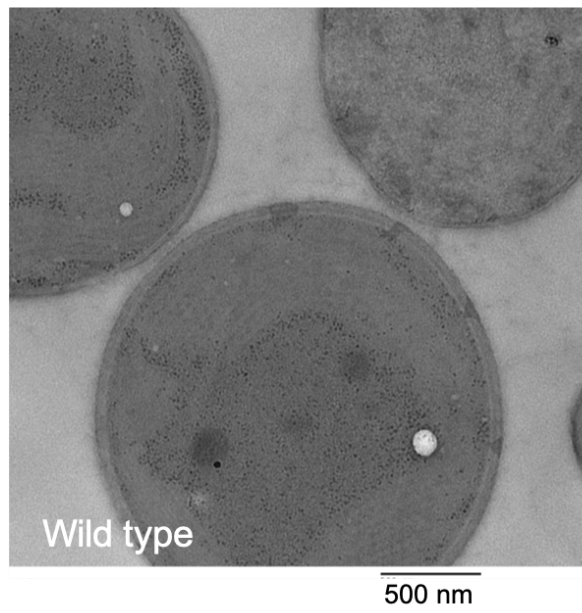
Supplementary Figure 4 Transmission electron micrograph of wild type cells and surface-layer

knock out cells. Scale bar 500 nm.
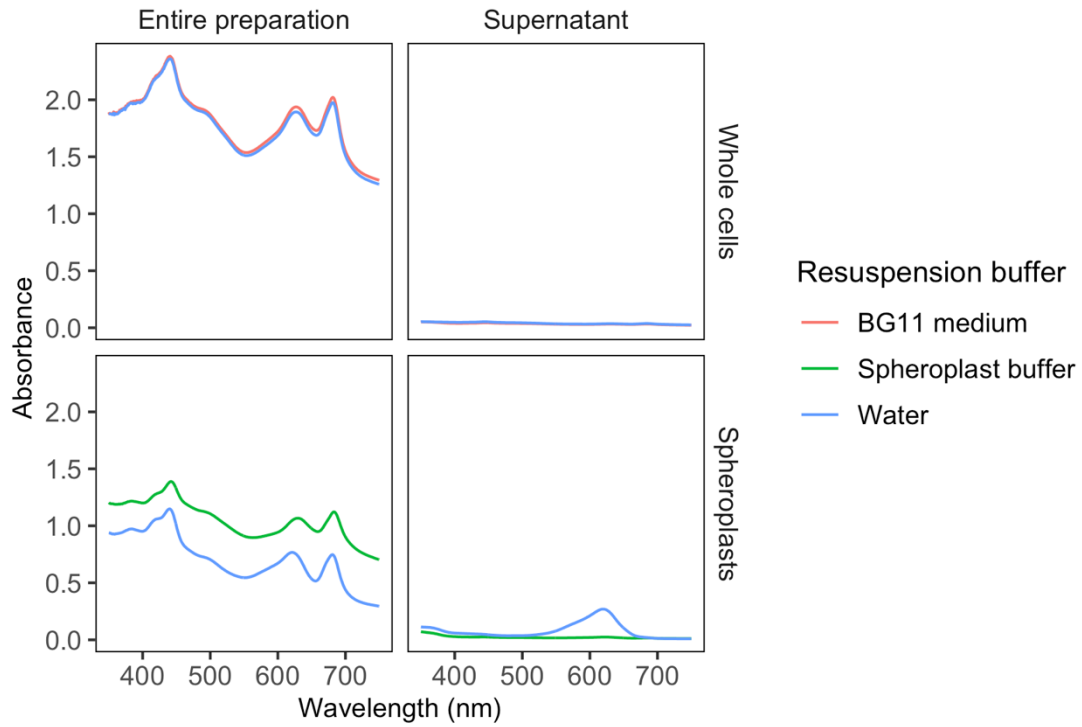
Supplementary Figure 5 UV-Vis spectra of spheroplast preparations from 350 to 750 nm. Rows: whole cell and spheroplast preparations. Columns: entire preparation or the supernatant after centrifugation at 3000 g for 7 min. Samples were resuspended in either buffer appropriate for that fraction (BG11 medium for whole cells, or spheroplast buffer for spheroplasts) or water. Phycocyanin absorbs at a λ_{max} = 622 nm.
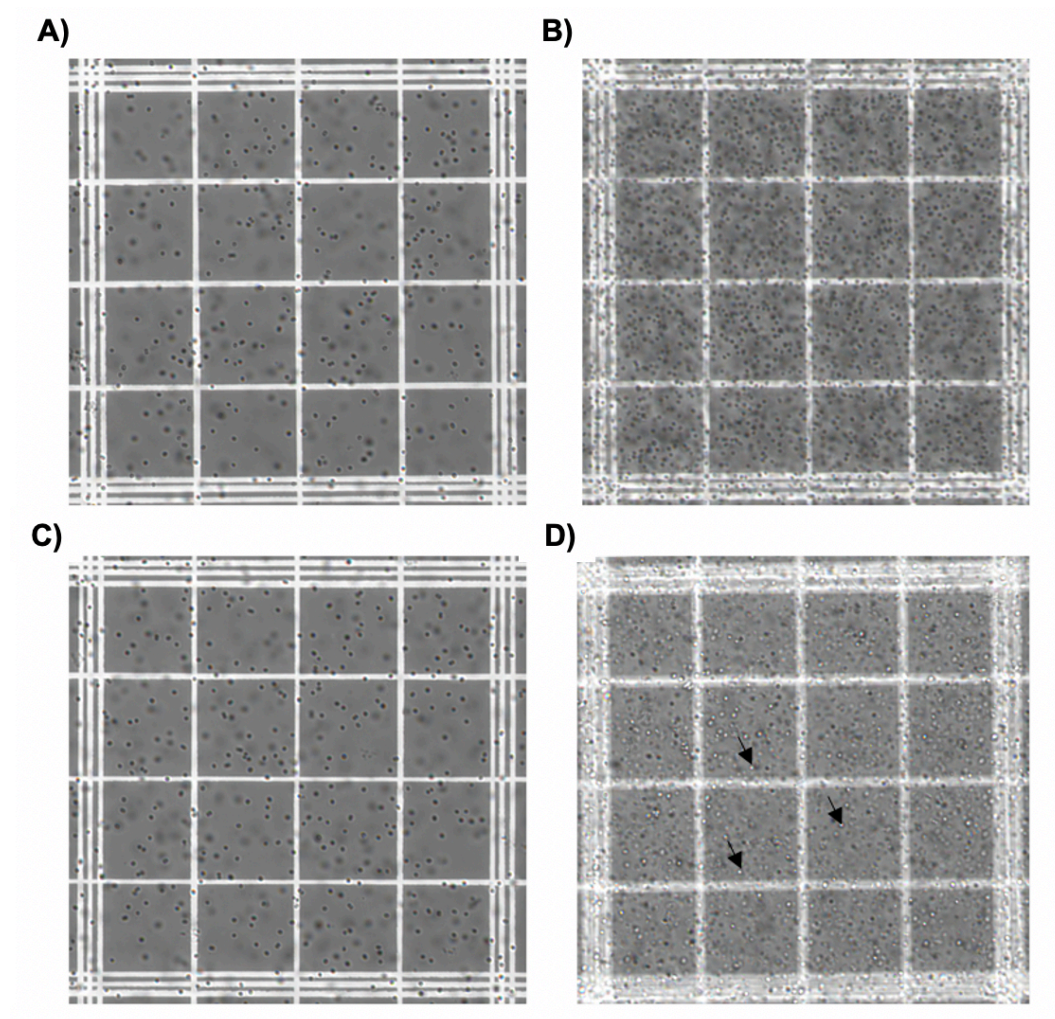
Supplementary Figure 6 Light microscope images of spheroplast preparations at 20 x magnification of (A, C) whole cell 1/100 x dilution, and (B, D) spheroplast 1x preparations in (A, B) appropriate buffer (BG11 and spheroplast buffer, respectively) and (C, D) water. Some spheroplast 'ghosts' are indicated with arrows.
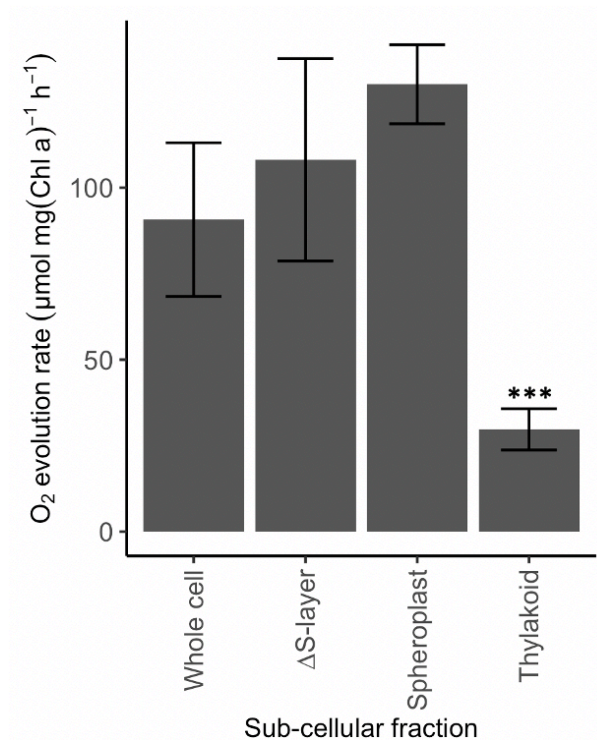
Supplementary Figure 7 Oxygen evolution rates of different sub cellular fractions from Clark Electrode measurements using 1520 μmol photons m^{-2} s^{-1} light at 627 nm, 1 mM DCBQ and 1 mM potassium ferricyanide. The electrolyte for whole wild-type cells and surface-layer mutant cells (ΔS-layer) was BG11 medium (pH 8.5); the electrolyte for spheroplasts was 10 mM HEPES buffer with 10 mM $MgCl_2$, 5 mM sodium phosphate and 0.5 M sorbitol (pH 7.5); and the electrolyte for isolated thylakoids was 50 mM MES buffer with, 15 mM NaCl, 5 mM $MgCl_2$, 2 mM CaCl2 (pH 6.0). Data presented as the mean of three biological replicates, error bars are standard error in the mean, *** = $P < 0.001$ compared to whole cell using a one way ANOVA and Tukey post-hoc test.

**Supplementary Table 2** Key properties of buffers of each subcellular fraction

Subcellular fraction	Buffer	Osmolarity	pH	Buffering	Redox active species
Wild-type cells and mutant cells (ΔS-layer and pilus mutants)	BG11 medium	58 mosmol	8	175.1 µM phosphate buffer	Mg^{2+}, citric acid, Mn^{2+}, Zn^{2+}, MoO_4^{2+}, Cu^{2+}, Co^{2+}, ferric citrate
Spheroplast	Spheroplast buffer	575 mosmol	7.5	10 mM HEPES	Mg^{2+}
Thylakoid membranes	Thylakoid buffer	121 mosmol	6.0	50 mM MES	Mg^{2+}
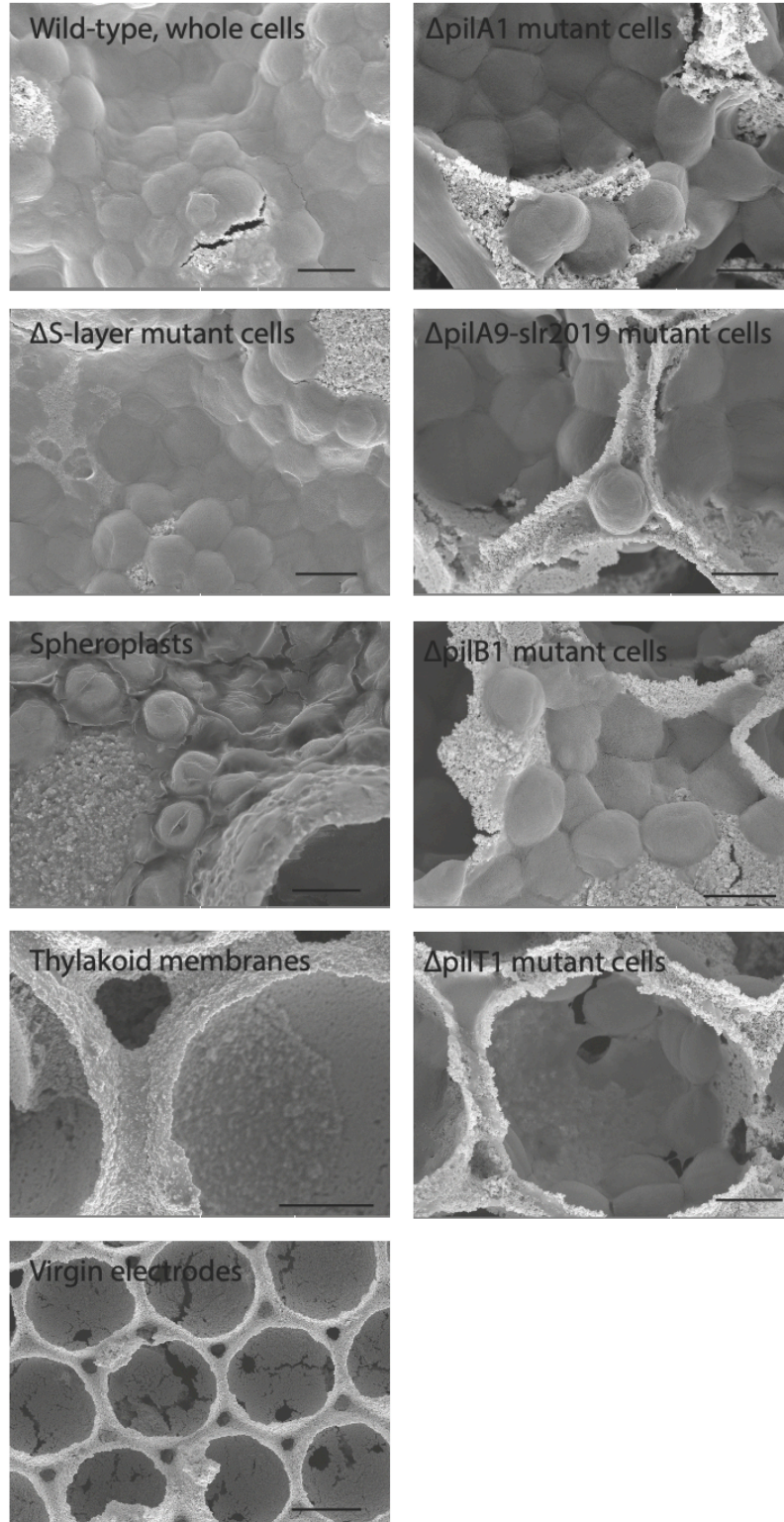
Supplementary Figure 8 Scanning electron microscope images of sub-cellular fractions of

Synechocystis loaded on IO-ITO electrodes according to the protocol for photoelectrochemistry. Scale

bar is 2 μm, apart from the virgin electrodes where the scale bar is 5 μm.
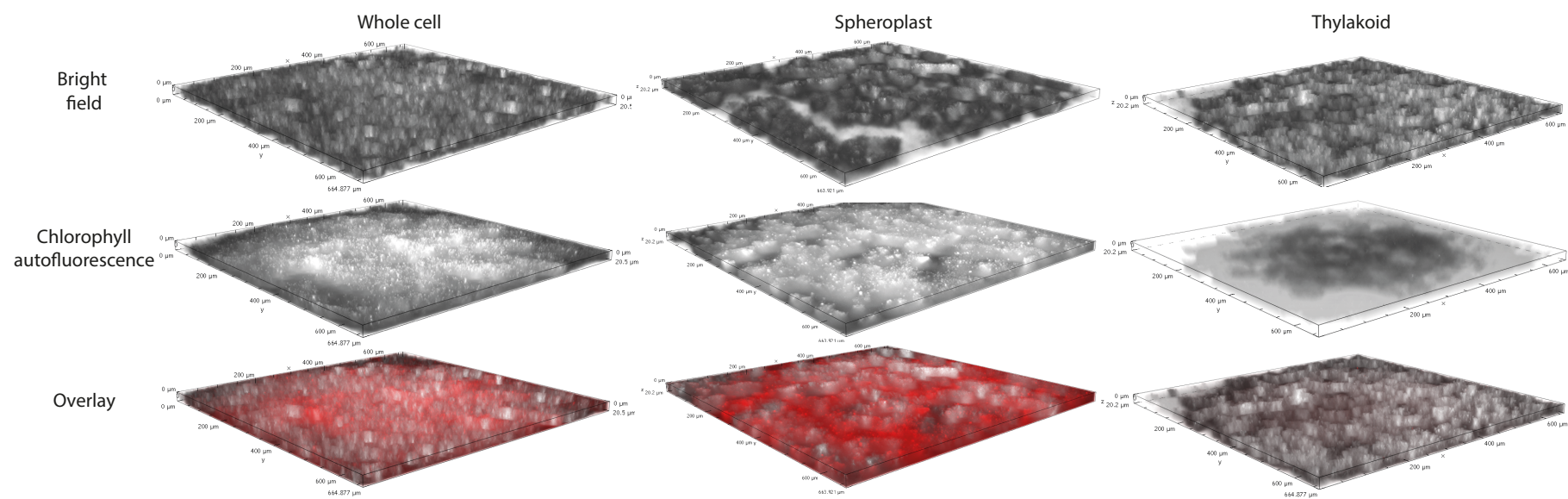
Supplementary Figure 9 3D visualisation of the sub-cellular fractions of *Synechocystis* integration and distribution within IO−ITO electrodes. The 3D view was reconstructed from Z-stacking images that were acquired by scanning 20 μm upward from the electrode base. Excitation: λex = 635 nm. Emission: λem = 690 nm.
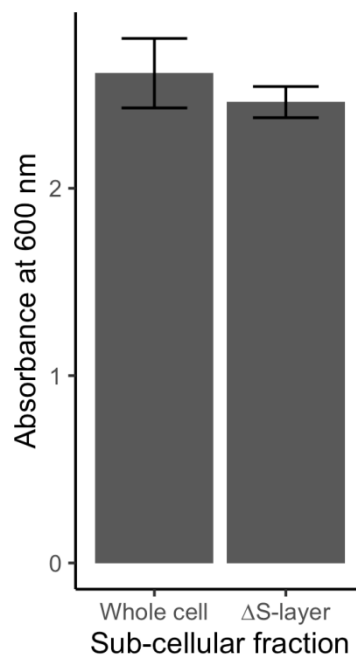
Supplementary Figure 10 Crystal violet assay of *Synechocystis* wild-type, whole cells and surface layer mutant cells (ΔS-layer). All loaded on ITO-PET. Data presented as the mean of four biological replicates, error bars are standard deviation, with no statistically significant difference using a one way ANOVA and Tukey HSD.

To confirm the difference in whole cell and spheroplast photocurrent profiles was not due to the different electrode loading techniques, whole cells were loaded on an electrode as per the spheroplast protocol and the photocurrent profile was measured. Whole cells still yielded a complex photocurrent profile under these conditions (**Supplementary Fig. 11**), although the features were less prominent than the features of the photocurrent profile of whole cells loaded 16 h before photoelectrochemistry experiments (**Fig. 2C**). Spheroplasts loaded on an electrode for 16 h before photoelectrochemical analysis showed complete loss of exoelectrogenic activity. It was found that leaving the thylakoid membrane preparation on the electrodes for longer than 20 min before photoelectrochemistry experiments yielded minimal photocurrent output with the sample appearing desiccated on the electrode.
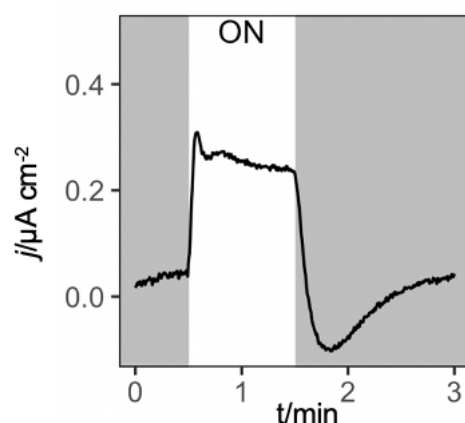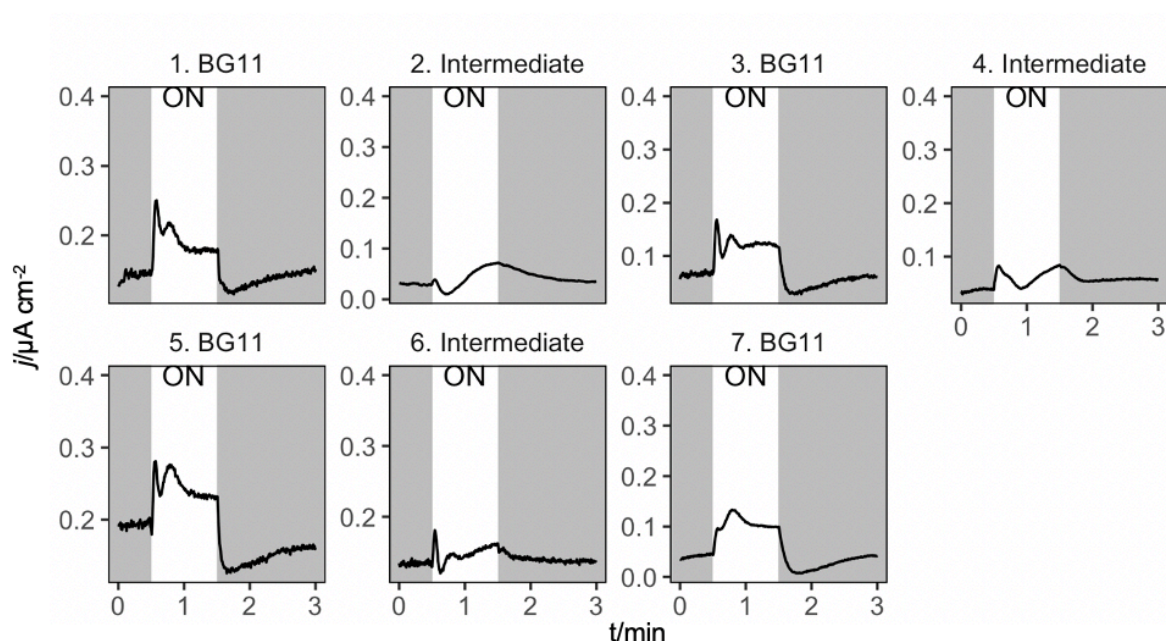

Supplementary Figure 11 Photocurrent profile of whole wild-type *Synechocystis* cells loaded for 1 h as for spheroplasts. Chronoamperometry measurements were recorded at an applied potential of 0.3 V vs. SHE, and under atmospheric conditions at 25 °C in BG11 medium electrolyte. Light conditions used: λ = 680 nm, 50 µmol photons m^{-2} s^{-1} (approximately 1 mW cm^{-2} equivalent). ON, light on. Data show one biological sample, presented as the mean of three consecutive light/dark cycles.

To confirm the difference in whole cell and spheroplast photocurrent profiles (complex versus monophasic, respesctive) was not due to the different electrolytes (**Supplementary**

Table 2), the photocurrent profile of whole cells was recorded in electrolytes with properties intermediate between BG11 medium and spheroplast buffer. Whole cells still yielded a complex photocurrent profile in intermediate electrolytes (**Supplementary Fig. 12**). However, the kinetics of the features of the photocurrent profiles were different in intermediate electrolytes. For example, in a 1/10 dilution of spheroplast buffer, which lacked the trace metal mixture (except for magnesium) in BG11 medium that is hypothesised to be involved exoelectrogenesis,[10] whole *Synechocystis* cells yielded a complex photocurrent profile with a large trough during the light period that was reminiscent of the photocurrent profile from *Synechococcus* cells in BG11 medium (**Supplementary Fig. 12** panel 2 and **Fig. 2B**). The exact reason for the difference in photocurrent profiles in intermediate electrolytes remains to be determined and will be the subject of future studies aiming to identify the role of individual components of the periplasmic space in exoelectrogenesis.

Incubation of whole cells in electrolyte identical to that used for spheroplasts led to complete loss of exoelectrogenic activity, necessitating the use of buffers with intermediate properties (**Supplementary Fig. 13**). Incubation of spheroplasts in electrolyte identical to that used for whole cells and buffers with intermediate properties led to complete loss of exoelectrogenic activity.

Supplementary Figure 12 Photocurrent profiles of whole wild-type cells transferred into different electrolytes. Number indicates the order in which the chronoamperometry experiments were performed. Electrolytes tested were: (1,3,5,7) BG11 medium (pH 8.5); (2) a 1/10 dilution of spheroplast buffer (10 mM HEPES buffer with 10 mM $MgCl_2$, 5 mM sodium phosphate and 0.5 M sorbitol (pH 7.5)) in water, which has the components of spheroplast buffer and the osmolarity of BG11 medium; (4) BG11 medium with 10 mM HEPES (pH 8.5), which has the pH of original BG11 medium and the buffering capacity of spheroplast buffer; and (6) BG11 medium with 10 mM HEPES (pH 7.5), which has the pH and buffering capacity of spheroplast buffer. Chronoamperometry measurements were recorded at an applied potential of 0.3 V vs. SHE, and under atmospheric conditions at 25 °C. Light conditions used: λ = 680 nm, 50 µmol photons m^{-2} s^{-1} (approximately 1 mW cm^{-2} equivalent). ON, light on. Data one biological sample, presented as the mean of three consecutive light/dark cycles.
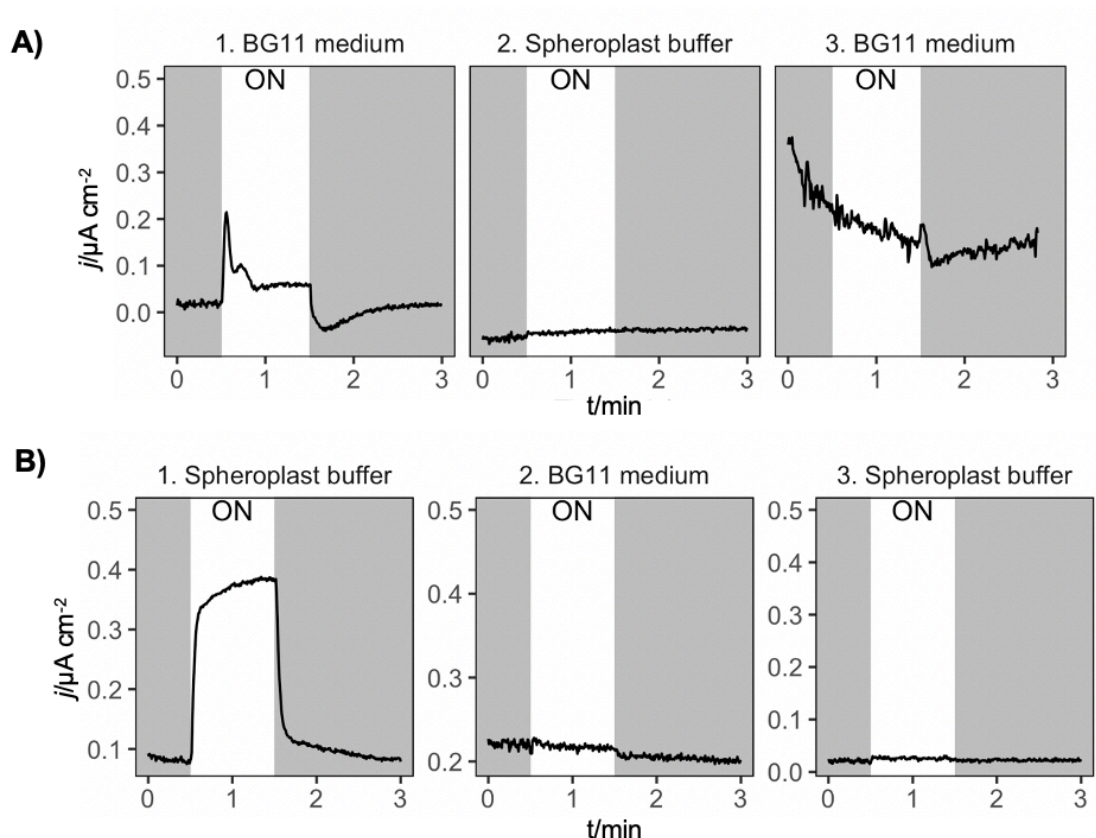
Supplementary Figure 13 Photocurrent profile in different electrolytes of **A)** whole wild-type cells and

B) spheroplasts. Number indicates the order in which the chronoamperometry experiments were

performed. Chronoamperometry measurements were recorded at an applied potential of 0.3

V vs. SHE, and under atmospheric conditions at 25 °C. Light conditions used: λ = 680 nm, 50 μmol

photons m^{-2} s^{-1} (approximately 1 mW cm^{-2} equivalent. ON, light on. Data one biological sample,

presented as the mean of three consecutive light/dark cycles

Supplementary Table 3 Primers used in this study for confirmation of the pilus mutants.

Primer	Sequence (5' to 3')
pilA1_screen_F	ATAACCAACTAAATCTCTGG
pilA1_screen_R	GGTAAGTTACAGCTAGAAGG
pilA9-slr2019_screen_F	AATTTGACTAGCAATAGTCC
pilA9-slr2019_screen_R	GACCAACATACTGTAACTGC
pilT1_screen_F	AAGAATAGTACCGAATTAGC
pilT1_screen_R	ATGTTAATCGGTATATTTCC
pilB1_screen_F	GGACAGTGGAATGTCCCCCA
pilB1_screen_R	GTGGTTCAATGTCGGCAAAA

Supplementary Table 4 Combination of primers and their expected sizes for confirmation of the pilus mutants.

Strain tested + primers used	Expected size (bp)
WT + ΔpilA1 primers	1481
ΔpilA1 + ΔpilA1 primers	1724
WT + ΔpilA9-slr2019 primers	6562
ΔpilA9-slr2019 + ΔpilA9-slr2019 primers	1821
WT + ΔpilT1 primers	1700
ΔpilT1 + ΔpilT1 primers	1521
WT + ΔpilB1 primers	2654
ΔpilB1 + ΔpilB1 primers	2084

Supplementary Table 5 Primers used in this study for generation and confirmation of the surface-layer

mutant.

Primer	Sequence (5' to 3')
Slayer_screen_F	GTCACGGCTACCGATGATCT
Slayer_ screen_R	CCGAGGCTGTTATCGTCAAT
Sll1951leftfor	GATCGAATTCGTCTTTGCCAAGCTGGAATC
Sll1951leftrev	GATCGGATCCGAAATTCGGGTCGTTCAAGA
Sll1951rightfor	GATCGGATCCGGGAAAATGGTATTGATG
Sll1951rightrev	GATCTCTAGATAACTTGATCGCTGGTGCTG

References

[1]   D.J. Lea-Smith, P. Bombelli, R. Vasudevan, C.J. Howe, Photosynthetic, respiratory and
       extracellular electron transport pathways in cyanobacteria, Biochim. Biophys. Acta -
       Bioenerg. 1857 (2016) 247–255. https://doi.org/10.1016/j.bbabio.2015.10.007.

[2]   D.J. Lea-Smith, G.T. Hanke, Electron Transport in Cyanobacteria and Its Potential in
       Bioproduction, in: J. Nielsen, S. Lee, G. Stephanopoulos, P. Hudson (Eds.), Cyanobacteria
       Biotechnol., 1st ed., Wiley, 2021: pp. 33–63. https://doi.org/10.1002/9783527824908.ch2.

[3]   L.T. Wey, P. Bombelli, X. Chen, J.M. Lawrence, C.M. Rabideau, S.J.L. Rowden, J.Z. Zhang,
       C.J. Howe, The Development of Biophotovoltaic Systems for Power Generation and
       Biological Analysis, ChemElectroChem. 6 (2019) 5375–5386.
       https://doi.org/10.1002/celc.201900997.

[4]   J.G.K. Williams, [85] Construction of specific mutations in photosystem II photosynthetic
       reaction center by genetic engineering methods in Synechocystis 6803, Methods Enzymol.
       167 (1988) 766–778. https://doi.org/10.1016/0076-6879(88)67088-1.

[5]   D.J. Lea-Smith, R. Vasudevan, C.J. Howe, Generation of marked and markerless mutants in
       model cyanobacterial species, J. Vis. Exp. 2016 (2016) 540013791–54001.
       https://doi.org/10.3791/54001.

[6]   H. Mi, T. Endo, U. Schreiber, T. Ogawa, K. Asada, NAD(P)H dehydrogenase-dependent
       cyclic electron flow around photosystem I in the cyanobacterium synechocystis PCC 6803: A
       study of dark-starved cells and spheroplasts, Plant Cell Physiol. 35 (1994) 163–173.
       https://doi.org/10.1093/oxfordjournals.pcp.a078580.

[7]   J. Komenda, J. Barber, Comparison of psbO and psbH Deletion Mutants of Synechocystis
       PCC 6803 Indicates that Degradation of D1 Protein Is Regulated by the QB Site and
       Dependent on Protein Synthesis, Biochemistry. 34 (1995) 9625–9631.
       https://doi.org/10.1021/bi00029a040.

[8]   F.D. Conradi, R.Q. Zhou, S. Oeser, N. Schuergers, A. Wilde, C.W. Mullineaux, Factors

controlling floc formation and structure in the cyanobacterium Synechocystis sp. strain PCC

6803, J. Bacteriol. 201 (2019) e00344-19. https://doi.org/10.1128/JB.00344-19.

[9]   T. Wallner, L. Pedroza, K. Voigt, V. Kaever, A. Wilde, The cyanobacterial phytochrome 2

regulates the expression of motility-related genes through the second messenger cyclic di-

GMP., Photochem. Photobiol. Sci. 19 (2020) 631–643. https://doi.org/10.1039/c9pp00489k.

[10]   B. Lai, H. Schneider, J. Tschörtner, A. Schmid, J.O. Krömer, Technical-scale biophotovoltaics

for long-term photo-current generation from Synechocystis sp. PCC6803, Biotechnol. Bioeng.

(2021). https://doi.org/10.1002/bit.27784.